

Intra-plate gabbroic rocks of Permo-Triassic to Early-Middle Triassic dike-and-sill province of Chukotka (Russia)

Galina V. Ledneva¹, Boris A. Bazylev², Paul W. Layer³, Akira Ishiwatari⁴, Sergey D. Sokolov¹, Natalia N. Kononkova², Petr L. Tikhomirov⁵ and Maria S. Novikova^{1,5}

¹Geological Institute, RAS, 7, Pyzhevsky per., Moscow 119017, Russia; ledneva@ilran.ru

²V.I. Vernadsky Institute of Geochemistry and Analytical Chemistry, RAS, 19, Kosygin st., Moscow 119991, Russia; bazylev@geokhi.ru

³College of Natural Science and Mathematics, University of Alaska Fairbanks, Fairbanks, AK, 99775, USA; pwlayer@alaska.edu

⁴Center of NE Asian Studies, Tohoku University, Kawauchi 41 Aoba-ku, Sendai 980-8576 Japan; geoishw@cneas.tohoku.ac.jp

⁵Geologic Faculty of Moscow State University, Vorob'yovy Gory, Moscow 119991, Russia; petr_tikhomirov@mail.ru

ABSTRACT

In order to provide basic materials for geodynamic and tectonic reconstruction of the Arctic region, we investigated Permo-Triassic to Early-Middle Triassic gabbroic rocks of tabular bodies in shelf and continental slope sediments of eastern Chukotka. These rocks, which are here referred to as the Anyui dike-and-sill province, are represented by gabbro, Fe-Ti gabbro, and gabbroic diorite assumed to be cogenetic to each other. The rocks from different tabular bodies can be originated from variably differentiated portions of melts at similar pressure and temperature conditions. The rocks show geochemical features of crustally contaminated intra-plate basaltic lavas and are geochemically similar to Permo-Triassic continental plateau basalts of the platformal (or the trap) stage of the Siberian large igneous province.

INTRODUCTION

Permo-Triassic to Early-Middle Triassic gabbroic rocks of the Chukotka Peninsula are an object of high interest for the tectonic evolution of the Arctic region prior to the Amerasia basin opening. The locations and extent of these volcanic rocks provide constraints on the original position of the Arctic Alaska-Chukotka continental margin (the AACM) relative to the Siberian and Canadian Arctic continental margins. According to the counterclockwise rotation model based on correlation of the Mesozoic-Paleozoic stratigraphy along with magnetic and gravity anomalies in the Amerasia basin, the AACM was pivoted from the Canadian Arctic margin during the Amerasia basin opening by

ripping commenced in the Early Cretaceous (Grantz, et al., 1990; Lawver and Scotese, 1990; Lawver, et al., 2002). Other studies taken into account geological data along with distributions of detrital zircon SHRIMP ages from sandstones of Chukotka, Wrangel Island and Alaska, petrochemical and geochemical similarity of gabbroic rocks of Chukotka and the New Siberian Islands coeval to traps of the Siberian large igneous province (LIP) (Fig. 1a), argue a close proximity of the Chukotka part of the AACM to the Siberian margin (the Taimyr and Verkhoyansk areas) in the Permo-Triassic to Early-Middle Triassic time (Miller, et al., 2006; Kuz'michov and Pease, 2007).

The similarity of Permo-Triassic magmatism of the New Siberian Islands to the Siberian LIP is well substantiated by geological observations, age (252 ± 2 Ma, U-Pb TIMS ages of igneous zircons) and bulk major- and trace-element compositions (Kuz'michov and Pease, 2007); however, correlation of the New Siberian Islands to the AACM is doubted by some researchers.

In the Chukotka Peninsula, small intrusions, dikes and sills of gabbroic rocks are widespread in the Permian - lower Triassic and lower-middle Triassic shelf and continental slope sediments. In the western Chukotka they extend for ~350 km (the Keperveem and Raucha Uplifts); in central and eastern Chukotka they are traced to a distance of ~900 km (the vicinity of Cape Schmidt and the interflaves of the Amguema and Vel'may rivers and the Kolyuchinskaya Bay area) (Fig. 1b). These gabbroic rocks were recognized as parts of a large regional complex (Til'man and Sosunov, 1960; Gel'man, 1963) named as the Amguema-Anyui Igneous Province

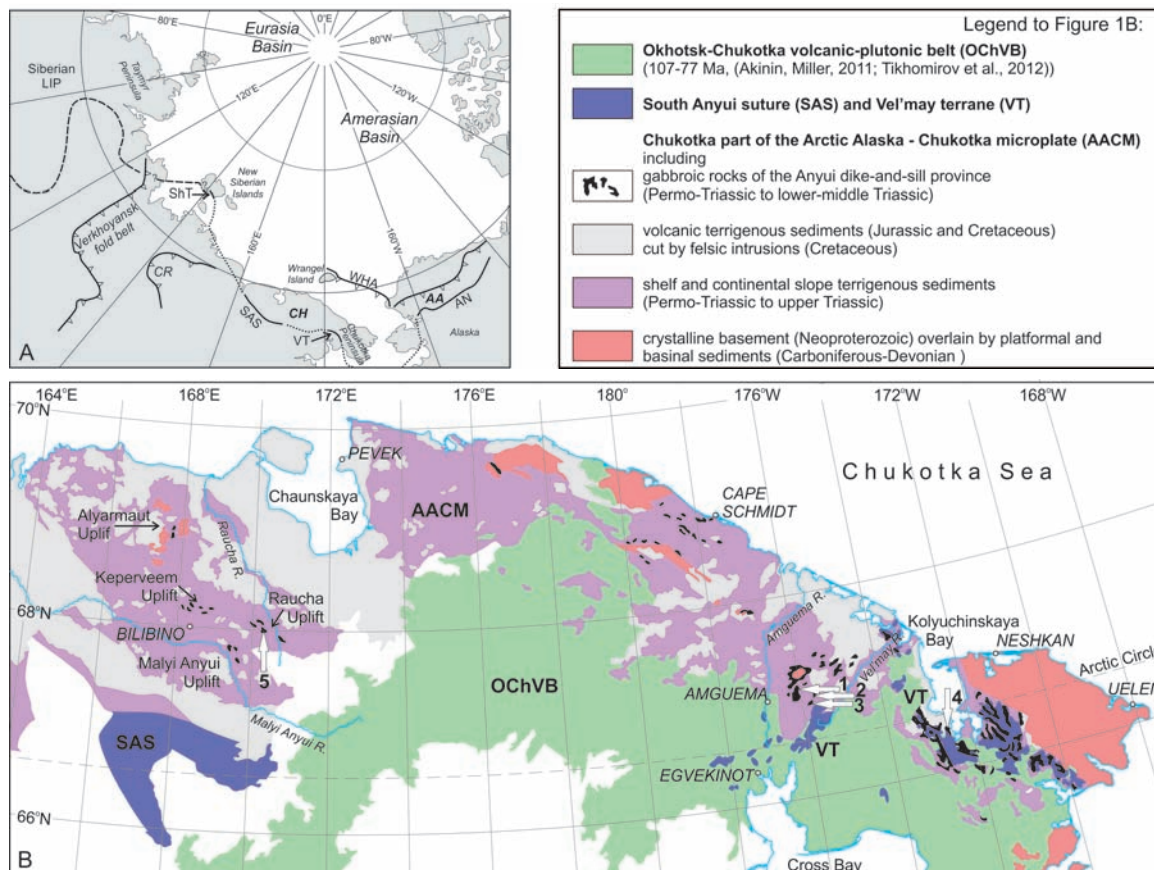


Fig. 1. Regional geological structures and locations of the studied gabbroic rocks of the Anyui dike-and-sill province.

(A) A position of the AACM among major geological structures of the Arctic region and adjacent areas (modified after Miller, et al., 2006). The AACM occupies Wrangel Island, the Chukotka (CH) and Arctic Alaska (AA) regions north of the Shalaurova terrane (ShT) in the New Siberian Islands, the South Anyui suture (SAS) in western Chukotka, the Vel'may terrane (VT) in eastern Chukotka, the Angayucham terrane (AN) in Alaska. The southern AACM boundary is shown in solid line and its inferred continuities are in the dotted line. The northern boundary of the AACM is supposedly marked by the Wrangel Herald Arch (WHA). The boundary of the Siberian LIP (dash line) is after Reichow, et al. (2009). CR is abbreviation for the Chersky Range.

(B) Sketch of the principle geological structures of Chukotka with localities of the domains investigated. The sketch is compiled using 1:2500000 geological map (Nalivkin, 1983); the Vel'may terrane is shown based on the geological scheme by Tynankergav and Bychkov (1987).

Locations of the rocks sampled and used for the comparison are shown by arrows. Numbers correspond to the domains as follows: the Gytgyl'ven pass (1), the Ploskaya River (2), Keeneyveem River (3), the Kolyuchinskaya Bay (4) and Bilibino (5).

by Degtyaryov (1975). In regional geological maps (scales 1:200000 and 1:1000000) these rocks were mapped as parts of a large regional complex referred to as the Anyui sill-and-dike series of gabbro-diorite or gabbro-dolerite. In this paper we will refer these gabbroic rocks to as the Anyui dike-and-sill province. Their Permo-Triassic to Early-Middle Triassic age is proven by their stratigraphic position within Permian - lower Triassic and lower-middle Triassic terrigenous sediments, joint deformation

of gabbroic bodies and their country rocks (Til'man and Sosunov, 1960; Gel'man, 1963), bulk-rock K-Ar determinations of 250, 231 and 223 Ma (Ivanov and Milov, 1975; Degtyaryov, 1975) and the U-Pb TIMS igneous zircon age of 252 ± 4 Ma obtained for the Kolyuchinskaya Bay gabbro (Sokolov, et al., 2009). Gel'man (1963) and Degtyaryov (1975) pointed out a similarity of bulk major-element composition of gabbroic rocks from western Chukotka (areas of the Keperveem, Malyi Anyui and Raucha Uplifts)

to continental tholeiitic basalts and Siberian trap basalts. The gabbro from the Kolyuchinskaya Bay area exhibit bulk-rock trace-element abundances, Rb-Sr and Sm-Nd isotope compositions indicative of their crystallization from variably differentiated portions of crustally contaminated basaltic magma. They are similar to intra-plate basalts in general and some tholeiitic basalts of the Siberian LIP in particular (Ledneva, et al., 2011).

Data on the Anyui dike-and-sill province of the Chukotka Peninsula are sparse and any regional correlations are speculative. In this paper we focus on characteristic of gabbroic rocks of the Anyui dike-and-sill province from several localities of eastern Chukotka. Rare samples from western Chukotka were investigated as well. We present new $^{40}\text{Ar}/^{39}\text{Ar}$ ages, major-element compositions of minerals and whole rocks, bulk-rock trace-element chemistry and Sm-Nd isotopes as well as their possible petrologic and geodynamic interpretations. This provides grounds for addressing the following issues:

- Were gabbroic rocks, which were distinguished as parts of the Anyui dike-and-sill province, generated in one magmatic event?
- Is there any connection between studied gabbroic rocks of the Chukotka Peninsula and coeval rocks of the New Siberian Islands?
- Can the Anyui dike-and-sill province be considered as a possible continuity of the Siberian LIP?

GEOLOGICAL SETTING

General geological and tectonic settings

The major tectonic units of the AACM (Fig.1b) are the Neoproterozoic crystalline basement (Bering Strait Geol. Field Party, 1997; Natal'in, et al., 1999; Cecile, et al., 1999; Amato, et al., 2009) and upper Paleozoic - Mesozoic sedimentary cover (Natal'in, et al., 1999; Tuchkova, et al., 2009). The basement is exposed in domes of high-grade metamorphic rocks that are intruded by Early Cretaceous granitoids and Late Cretaceous mafic to intermediate rocks (e.g. Bering Strait Geol. Field Party, 1997; Amato, et al., 1997, 2003; Dorofeev, et al., 1999; Layer, et al., 2001; Miller, et al., 2009; Tikhomirov, et al., 2009). The sedimentary cover comprises Carboniferous and Permian carbonate platform strata (Natal'in, et al., 1999), Permo-Triassic to upper Triassic terrigenous

continental slope and shelf sediments (Tuchkova, et al., 2009) and Jurassic volcanic-terrigenous foreland sediments (Vatrushkina and Tuchkova, 2014).

The southern boundary of the AACM is widely hidden under the Cretaceous (Albian-Cenomanian and Santonian-Campanian) Okhotsk-Chukotka volcanic belt (Akinin and Miller, 2011; Tikhomirov, et al., 2012). In western Chukotka it is marked by the South Anyui Suture, which originated via closure of an oceanic basin and collision of the ACCM with the Asian continental margin during the early Cretaceous (Seslavinsky, 1979; Fujita and Newberry, 1982; Parfenov, 1984; Parfenov, et al., 1993; Nokleberg, et al., 1998). In eastern Chukotka its position is less certain and ascribed to the Vel'may terrane (Parfenov, et al., 1993; Nokleberg, et al., 1998; Sokolov, et al., 2009).

Geological setting of rocks of the Anyui dike-and-sill province

Sampling locations are shown in Figure 1b and are listed in Table 1.

Gabbroic rocks of the Anyui dike-and-sill province form numerous tabular bodies from a few meters to a few hundred meters thick that are mainly confined to the upper Permian - lower Triassic and lower-middle Triassic strata of the AACM cover (see notes for Table 1). Upper Triassic sediments gradually overlying these older sequences are free of tabular bodies of gabbroic rocks (Til'man and Sosunov, 1960; Gel'man, 1963; Degtyaryov, 1975; authors' observations). In Paleozoic limestones underlying Permo-Triassic and Triassic sediments elongated diabase lenses of a few hundred meters long and a few meters thick were described by Gel'man (1963).

In the study areas, gabbroic rocks are commonly exposed as eluvium and diluvium deposits due to frost weathering. In talus, fresh or relatively fresh gabbroic rocks are often mixed up with mudstones, siltstones, sandstones and bedded tuffs while metagabbros are intermixed with slates, schists and amphibolites. Bedrock exposures were investigated in domains of the Ploskaya River and Gyt'gylven pass. In the steep southern bank of the Ploskaya River gabbroic rocks constitute a sill of about 30 m thick and a body of unknown thickness (one of the contacts is covered with vegetation). Gabbros intrude

Table 1. List of samples and localities.

No	Sample	Rock group*	Rock name (based on petrographic description)	Domain **	Country rocks, Formation***	Longitude	Latitude	Type of exposure
1	GY9-74	Fe-Ti gabbro	metagabbro rich in Fe-Ti oxides	Gytgyl'ven pass (1)	Iul'tin, P-T ₁	178°11,404'W	67°09,543'N	bedrock
2	GY9-76	Fe-Ti gabbro	Qtz-bearing Hbl gabbro/diorite rich in Fe-Ti oxides	Gytgyl'ven pass (1)	Iul'tin, P-T ₁	178°11,514'W	67°09,741'N	eluvium
3	GY9-78	gabbroic diorite	Qtz diorite	Gytgyl'ven pass (1)	Iul'tin, P-T ₁	178°11,845'W	67°09,951'N	eluvium
4	GY9-79	Fe-Ti gabbro	metagabbro rich in Fe-Ti oxides	Gytgyl'ven pass (1)	Iul'tin, P-T ₁	178°11,845'W	67°09,951'N	eluvium
5	GY9-81	Fe-Ti gabbro	metagabbro rich in Fe-Ti oxides	Gytgyl'ven pass (1)	Iul'tin, P-T ₁	178°08,924'W	67°08,955'N	deluvium
6	GY9-82a	gabbroic diorite	diorite	Gytgyl'ven pass (1)	Iul'tin, P-T ₁	178°08,924'W	67°08,955'N	deluvium
7	GY9-82b	gabbroic diorite	Qtz diorite	Gytgyl'ven pass (1)	Iul'tin, P-T ₁	178°08,924'W	67°08,955'N	deluvium
8	GY9-84	gabbroic diorite	Qtz-metagabbro/Qtz-metadiorite	Gytgyl'ven pass (1)	Iul'tin, P-T ₁	178°09,677'W	67°08,952'N	deluvium
9	GY9-85	gabbroic diorite	Qtz diorite	Gytgyl'ven pass (1)	Iul'tin, P-T ₁	178°09,677'W	67°08,952'N	deluvium
10	GY9-87	gabbroic diorite	Qtz diorite	Gytgyl'ven pass (1)	Iul'tin, P-T ₁	178°10,161'W	67°08,932'N	deluvium
11	GY9-98	Fe-Ti gabbro	metagabbro rich in Fe-Ti oxides	Gytgyl'ven pass (1)	Iul'tin, P-T ₁	178°08,543'W	67°09,564'N	deluvium
12	GY9-99	Fe-Ti gabbro	Qtz-bearing Bi-Hbl gabbro rich in Fe-Ti oxides	Gytgyl'ven pass (1)	Iul'tin, P-T ₁	178°08,537'W	67°09,584'N	deluvium
13	GY9-101	gabbro	Qtz-bearing Hbl gabbro	Gytgyl'ven pass (1)	Iul'tin, P-T ₁	178°08,430'W	67°09,694'N	bedrock
14	GY9-102	Fe-Ti gabbro	metagabbro rich in Fe-Ti oxides	Gytgyl'ven pass (1)	Iul'tin, P-T ₁	178°08,329'W	67°09,726'N	bedrock
15	PS9-89	Fe-Ti gabbro	Qtz-bearing Bi-Hbl gabbro/diorite rich in Fe-Ti oxides	Ploskaya River (2)	Amguema, T ₁₋₂	177°52,958'W	67°07,954'N	bedrock
16	PS9-90	Fe-Ti gabbro	metagabbro/metadiorite rich in Fe-Ti oxides	Ploskaya River (2)	Amguema, T ₁₋₂	177°52,872'W	67°07,987'N	bedrock
17	PS9-92	gabbro	Qtz-bearing Bi-Hbl gabbro	Ploskaya River (2)	Amguema, T ₁₋₂	177°52,843'W	67°08,001'N	bedrock
18	KE9-71	Fe-Ti gabbro	Qtz diorite rich in Fe-Ti oxides	Keeneyveem River (3)	Amguema, T ₁₋₂	177°40,520'W	66°56,668'N	bedrock
19	KE9-72	Fe-Ti gabbro	Qtz-bearing Hbl gabbro rich in Fe-Ti oxides	Keeneyveem River (3)	Amguema, T ₁₋₂	177°40,520'W	66°56,668'N	bedrock
20	KE9-73	Fe-Ti gabbro	Qtz-bearing Bi-Hbl gabbro rich in Fe-Ti oxides	Keeneyveem River (3)	Amguema, T ₁₋₂	177°40,690'W	66°56,599'N	bedrock
21	P-11-7	gabbro	Qtz-bearing Hbl gabbro	Bilibino area (5)	Keperveem, T ₁₋₂	169°00,768'E	67°51,082'N	bedrock
22	P-11-7a	gabbro	Qtz-bearing Hbl gabbro (brecciated)	Bilibino area (5)	Keperveem, T ₁₋₂	169°00,768'E	67°51,082'N	bedrock
23	T-05-5	gabbro	Qtz-bearing Bi gabbro	Bilibino area (5)	Keperveem, T ₁₋₂	167°55,060'E	68°04,087'N	bedrock

* Rock group distinguished based on the bulk major-element composition of rocks.

** Numbers in the brackets correspond to the localities in Figure 1b.

*** The Iul'tin Formation is made of the upper Permian-lower Triassic strongly deformed slates, carbonaceous schists, siltstones and rare sandstones. The Amguema Formation (distinguished in eastern Chukotka) is represented by lower Triassic and lower-middle Triassic sequences of rhythmically bedded sandstones, calcareous siltstone and mudstones with calcareous concretions and rare intraformational conglomerates. The Keperveem Formation (recognized in western Chukotka) is facial analogues of the Amguema Formation (Explanatory notes to the regional geologic maps).

the folded sequence of bedded mudstones, siltstones and sandstones with rare thin layers of tuffs. Inner parts of the gabbroic bodies are composed of massive medium- and coarse-grained rocks without any features of magmatic banding. The sill has chilled contacts, which are marked by pinkish hornfels in the exocontact and very fine-grained gabbros in the endocontact. In the Gyt'gylven pass sills of a few meters to a few tens meters thick are embedded in strongly folded metamorphic rocks and are made of metagabbros. The sills are folded along with host slates and schists; and primary chilled contacts are often tectonically disrupted.

Similar geological relationships between gabbroic rocks of the Anyui dike-and-sill province were described in the Kolyuchinskaya Bay area in eastern Chukotka (Ledneva, et al., 2011) and in western Chukotka (Til'man and Sosunov, 1960; Gel'man, 1963; Degtyaryov, 1975). Gel'man (1963) also pointed out that in areas of the most intensive

deformations (for example the eastern flank of the Alyarmaut Uplift) tabular bodies are boudinaged. The boudins are traced for a distance of ~1-2.5 km and they are composed of amphibolites presumably originated after gabbroic rocks.

AGE

For ⁴⁰Ar/³⁹Ar analysis, samples were submitted to the Geochronology laboratory at the University of Alaska Fairbanks where they were crushed, sieved, washed and hand-picked for mineral phases. The monitor mineral MMhb-1 (Samson and Alexander, 1987) with an age of 513.9 Ma (Lanphere and Dalrymple, 2000) was used to monitor neutron flux (and calculate the irradiation parameter, J). The samples and standards were wrapped in aluminum foil and loaded into aluminum cans of 2.5 cm diameter and 6 cm height. The samples were irradiated in position 5c of the uranium enriched research reactor of McMaster University in Hamilton, Ontario, Canada

for 20 megawatt-hours. Upon their return from the reactor, the samples and monitors were loaded into 2 mm diameter holes in a copper tray that was then loaded in an ultra-high vacuum extraction line. The monitors were fused, and samples heated, using a 6-watt argon-ion laser following the technique described in York, et al. (1981), Layer, et al. (1987) and Layer (2000). Argon purification was achieved using a liquid nitrogen cold trap and a SAES Zr-Al getter at 40°C. The samples were analyzed in a VG-3600 mass spectrometer at the Geophysical Institute, University of Alaska Fairbanks. The argon isotopes measured were corrected for system blank and mass discrimination, as well as calcium, potassium and chlorine interference reactions following procedures outlined in McDougall and Harrison (1999). System blanks generally were 2×10^{-16} mol⁴⁰Ar and 2×10^{-18} mol³⁶Ar which are 10 to 50 times smaller than fraction volumes. Mass discrimination was monitored by running both calibrated air shots and a zero-age glass sample. These measurements were made on a weekly to monthly basis to check for changes in mass discrimination.

Results of ⁴⁰Ar/³⁹Ar dating

Results of the ⁴⁰Ar/³⁹Ar dating are shown in Table 2 and Figure 2. ⁴⁰Ar/³⁹Ar plateau ages obtained are 218.3 ± 5.2 Ma for hornblende of gabbroic diorite (sample GY9-87, the Gytgyl'ven pass) and 167.8 ± 11.2 Ma for actinolite with minor relicts of primary hornblende of Fe-Ti gabbro (sample PS9-89, the Ploskaya River).

PETROGRAPHY

Studied rocks of the Anyui province can be divided into three broad groups comprising the gabbro, Fe-Ti gabbro and gabbroic diorite. Each group includes rocks that are metamorphosed to a different extent, so some samples investigated are actually metagabbro and metadiorite. Rock names and groups to which they were attributed are given in Table 1. Relicts of primary silicates occupy usually only central parts of some grains with rims being pseudomorphed by metamorphic minerals. The petrographic description is based mainly on relatively fresh samples. In general, the original modal contents of mafic minerals in the rocks are

Table 2. Results of the argon measurements.

GY9-87 hornblende																
Weighted average of J from standards = $3.624 \times 10^{-3} \pm 1.367 \times 10^{-5}$																
Laser (mW)	Cum. ³⁹ Ar	⁴⁰ Ar/ ³⁹ Ar meas.	±	³⁷ Ar/ ³⁹ Ar meas.	±	³⁶ Ar/ ³⁹ Ar meas.	±	% Atm ⁴⁰ Ar	Ca/K	±	Cl/K	±	⁴⁰ Ar*/ ³⁹ Ar _K	±	Age (Ma)	± (Ma)
400	0,0114	855,459	20,608	4,1314	0,0816	2,7331	0,0598	94,4	7,60	0,15	0,0787	0,0041	48,268	22,689	290,9	126,3
800	0,0412	330,984	9,418	4,8920	0,1374	1,0068	0,0258	89,8	9,01	0,25	0,0711	0,0028	33,978	8,363	209,5	48,7
1200	0,0745	260,902	6,582	6,0898	0,1285	0,7745	0,0160	87,5	11,22	0,24	0,0900	0,0024	32,638	6,311	201,7	36,9
1500	0,1013	195,822	5,409	5,0209	0,1213	0,5534	0,0146	83,3	9,25	0,22	0,1817	0,0053	32,793	5,112	202,6	29,9
1750	0,1268	157,683	4,153	6,3412	0,1725	0,4268	0,0122	79,7	11,69	0,32	0,2259	0,0059	32,211	4,198	199,2	24,6
2000	0,1606	112,396	3,274	6,1122	0,2006	0,2748	0,0100	71,8	11,26	0,37	0,3395	0,0103	31,815	3,449	196,9	20,2
3000	0,2845	83,216	1,975	7,9697	0,1475	0,1640	0,0036	57,5	14,71	0,27	0,5429	0,0089	35,591	1,971	218,9	11,4
5000	0,6215	73,123	1,669	7,6599	0,1241	0,1294	0,0024	51,4	14,13	0,23	0,5915	0,0087	35,683	1,650	219,4	9,6
9000	1,0000	59,303	1,382	9,2375	0,1418	0,0808	0,0015	39,0	17,06	0,26	0,6228	0,0103	36,385	1,332	223,5	7,7
Integrated		98,714	0,987	7,9648	0,0692	0,2163	0,0018	64,1	14,70	0,13	0,5304	0,0048	35,632	0,916	219,1	5,4
PS9-89 actinolite																
Weighted average of J from standards = $3.624 \times 10^{-3} \pm 1.367 \times 10^{-5}$																
Laser (mW)	Cum. ³⁹ Ar	⁴⁰ Ar/ ³⁹ Ar meas.	±	³⁷ Ar/ ³⁹ Ar meas.	±	³⁶ Ar/ ³⁹ Ar meas.	±	% Atm ⁴⁰ Ar	Ca/K	±	Cl/K	±	⁴⁰ Ar*/ ³⁹ Ar _K	±	Age (Ma)	± (Ma)
500	0,0905	506,866	14,995	8,5942	0,2966	1,6044	0,0514	93,4	15,87	0,55	0,0643	0,0036	33,660	13,623	207,7	79,4
750	0,1800	309,578	10,015	5,9250	0,2207	0,9391	0,0335	89,5	10,92	0,41	0,0507	0,0030	32,672	8,571	201,9	50,1
1000	0,2852	135,433	7,947	4,0961	0,2189	0,3698	0,0210	80,5	7,54	0,40	0,0462	0,0032	26,535	7,340	165,7	43,8
1500	0,4383	100,217	5,657	5,9873	0,3128	0,2463	0,0130	72,1	11,03	0,58	0,0626	0,0039	28,029	4,989	174,6	29,6
1750	0,5362	74,323	5,342	7,7837	0,5235	0,1713	0,0132	67,3	14,36	0,97	0,0575	0,0046	24,450	4,925	153,2	29,6
2250	0,6783	54,138	3,369	8,2545	0,5254	0,0998	0,0072	53,2	15,23	0,98	0,1243	0,0084	25,455	3,049	159,2	18,3
2750	0,7714	58,484	2,993	12,4592	0,6529	0,1154	0,0074	56,6	23,06	1,22	0,0755	0,0045	25,602	3,054	160,1	18,3
4000	0,9011	64,572	2,910	23,8160	1,1043	0,1245	0,0064	54,0	44,45	2,10	0,1200	0,0056	30,218	2,809	187,5	16,6
5000	0,9647	70,458	3,485	29,6883	1,3706	0,1384	0,0079	54,6	55,64	2,62	0,1934	0,0094	32,672	3,513	201,9	20,5
9000	1,0000	151,887	7,049	96,9457	4,3119	0,3650	0,0172	65,8	190,96	9,12	0,2022	0,0097	55,812	7,032	332,4	38,2
Integrated		141,615	2,308	14,3797	0,2633	0,3846	0,0067	79,4	26,66	0,49	0,0901	0,0018	29,415	2,012	182,8	11,9

impossible to evaluate from petrography.

Gabbro and Fe-Ti gabbro are massive fine- to medium-grained rocks of hypidiomorphic-granular texture (Fig. 3a). The rocks are mainly composed of hornblende, augite, plagioclase, ilmenite, and Ti-magnetite, and contain variable amounts of biotite, accessory apatite and sodium-potassium

feldspars, trace micrographic intergrowths of quartz with orthoclase and albite (or discrete grains of these minerals) and sulfides. Minor pigeonite and orthopyroxene are present only in a few samples studied. Mafic silicates are dominated by hornblende. The exception is sample T05-5, which seems to be hornblende-free. The plagioclase content in the

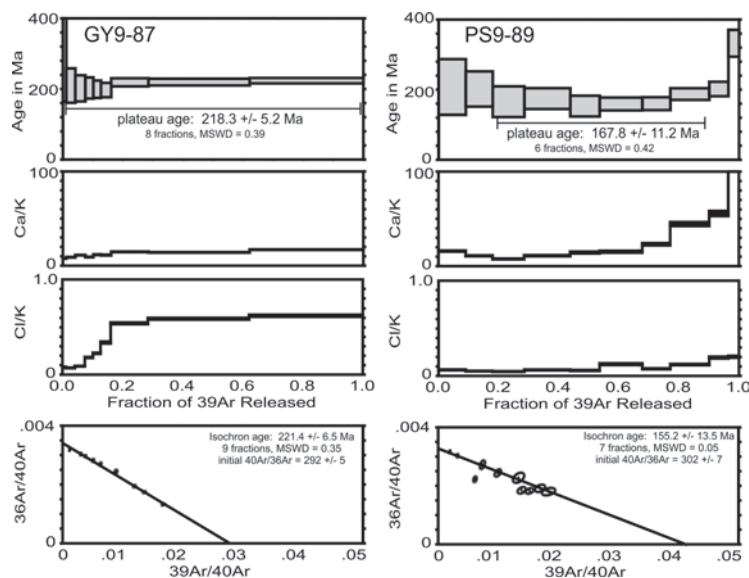


Fig 2. Age, Ca/K and Cl/K spectra and correlation diagrams for hornblende and actinolite. Plateau and isochron ages are indicated. MSWD: Mean square weighted deviations, a measure of plateau or isochron scatter.

Fig. 3. Photomicrographs and back-scattered electron (BSE) images demonstrating typical textures and other features of rocks of the Anyui province. Acronyms are as follows: Ab – albite, Afs – alkali feldspars, Amph – amphibole, Ano – anorthoclase, Ap – apatite, Aug – augite, Chl – chlorite, Ep – epidote, Hbl – hornblende, Ilm – ilmenite, Pl – plagioclase, rTi-Mag – Ti-magnetite pseudomorphly replaced by titanite, Stil – stilpnomelane, Ti-Mag – Ti-magnetite, Ttn – titanite, Qtz – quartz.

(a) Massive hypidiomorphic-granular Fe-Ti gabbro (sample KE9-73) dominated by euhedral crystals of zoned feldspars and subhedral grains of hornblende and augite; quartz and micrographic intergrowths of quartz with alkali feldspar fills interstices and constitute less than 2-3 %. Primary hornblende is partially replaced by actinolite. Cross-polarized light.

(b) BSE image showing zonation of euhedral feldspar grains and details of granophyric groundmass of Fe-Ti gabbro (sample PS9-89). The core of feldspar grain is composed of labradorite (An53); the inner and outer rims are made of oligoclase (An36) and anorthoclase, respectively. Groundmass is dominated by micrographic intergrowths of anorthoclase, albite and quartz and individual grains of orthoclase and quartz.

(c) Massive hypidiomorphic-granular Fe-Ti gabbro with micrographic groundmass (sample PS9-89). The rock is made of euhedral crystals of zoned feldspars, subhedral grains of hornblende merged in the groundmass of intergrown quartz, albite and orthoclase. Cross-polarized light.

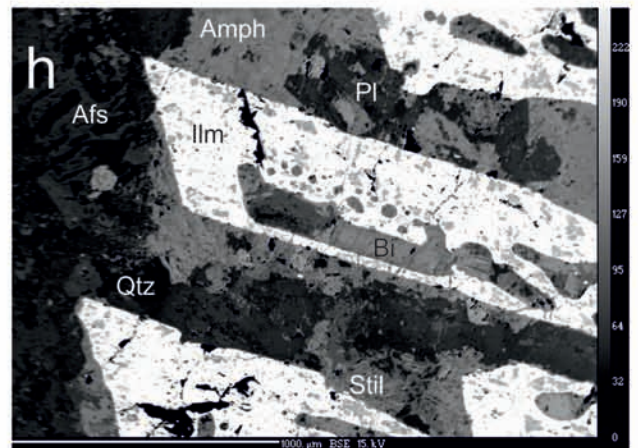
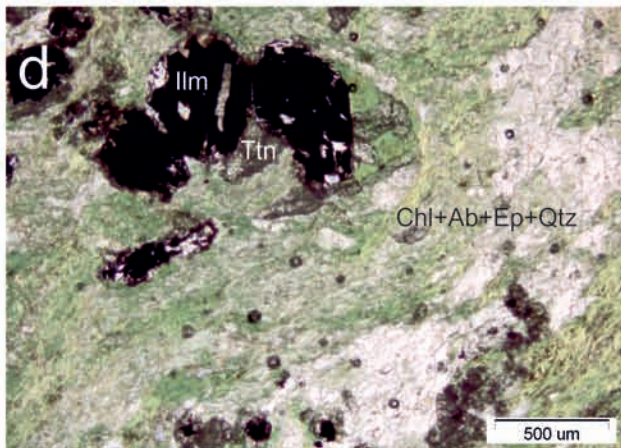
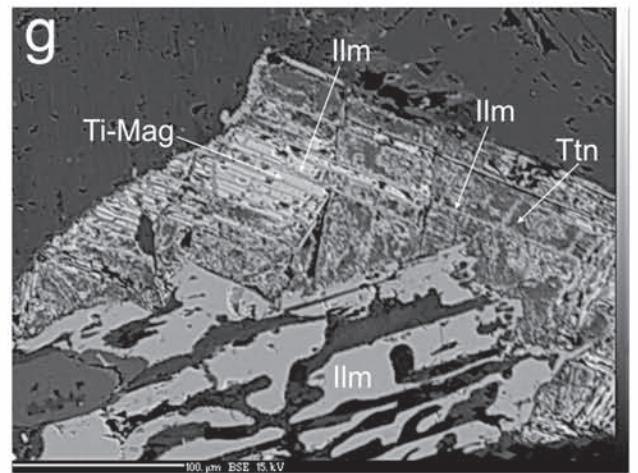
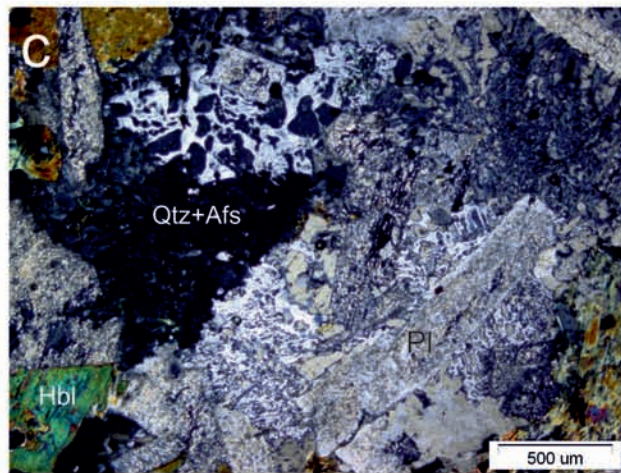
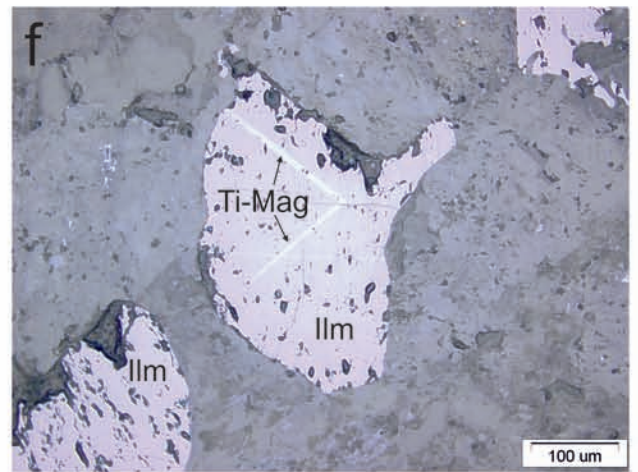
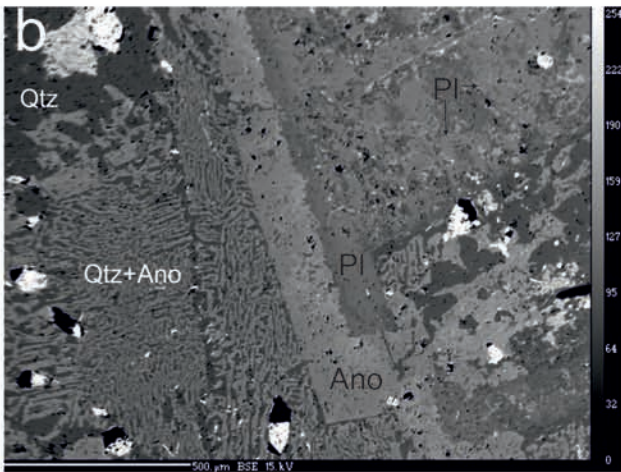
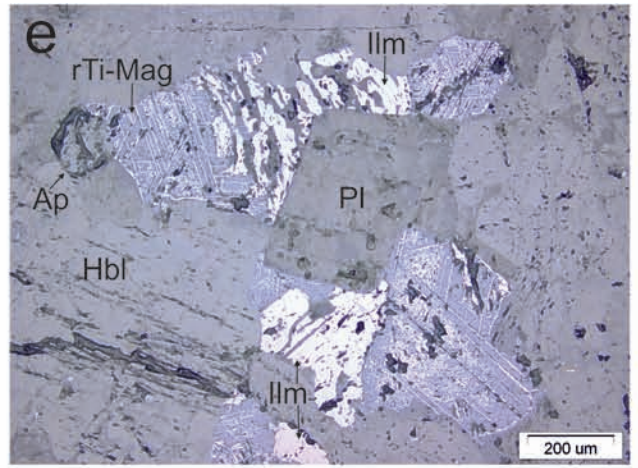
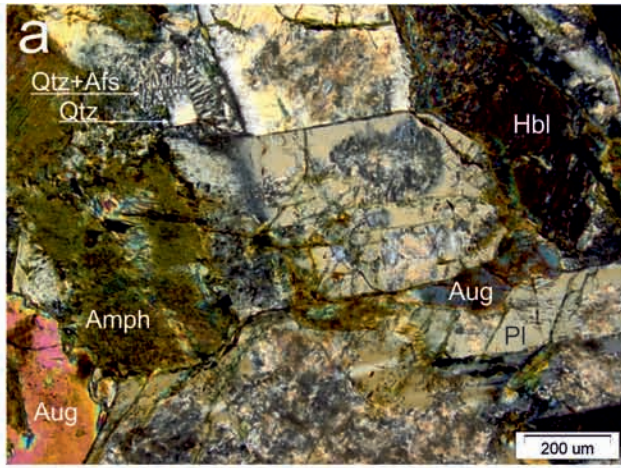
(d) Metagabbro presumably resulted from nearly complete metamorphic alteration of a gabbro (sample GY9-102). A primary texture is not preserved; metamorphic minerals are chlorite, albite, quartz, epidote, and titanite. Titanite and high-Mn ilmenites form pseudomorphs after primary Ti-magnetite and ilmenite. This rock contains only very rare relicts (a few to a few tens microns) of hornblende similar in composition to a primary one (Table 3). Plane-polarized light.

(e) Ilmenite grains and pseudomorphs of titanite after Ti-magnetite with preserved ilmenite lamellae in Fe-Ti gabbro (sample KE9-71). Reflected light.

(f) Ti-magnetite lamellae in ilmenite, Fe-Ti gabbro (sample KE9-71). Reflected light.

(g) Ilmenite intergrown with Ti-magnetite with ilmenite lamellae, Ti-magnetite is partially replaced by titanite, Fe-Ti gabbro (sample KE9-71). BSE image.

(h) Euhedral grains of ilmenites with numerous inclusions of silicate minerals (biotite, amphibole and etc.), Fe-Ti gabbro (sample PS9-89). BSE image.



rocks amounts to 30-40%. The contents of Fe-Ti oxides is evaluated at 5-10% (the highest value is typical for the Fe-Ti gabbros); ilmenite dominates over Ti-magnetite with a factor of about 2.

Hornblende forms anhedral, subhedral, or euhedral elongated, or isometric grains and displays pleochroism from greenish to brown colors. Euhedral and subhedral grains, often occurring as aggregates, show only weak pleochroism, and anhedral grains in contact with quartz have stronger pleochroism. Augite forms isometric subhedral grains without a visible pleochroism. Pigeonite was found in trace amount only in two samples (GY9-73 and T-05-5), where it forms small (a few tens of microns) subhedral crystals completely or partially embedded in augite and biotite. Orthopyroxene was found only in one sample (T-05-5), in which it forms small subhedral grains embedded in augite. Augites in this sample contain exsolution lamellae of pigeonite and vice versa; other samples studied have no pyroxenes with exsolution lamellae. Biotite is pleochroic from dark to light reddish brown. It forms small euhedral laths included in Fe-Ti oxides and anhedral grains that fill interstices along with hornblende, quartz and Fe-Ti oxides. Plagioclase forms euhedral and subhedral tabular crystals displaying sometimes clear optical compositional zoning. Polysynthetic twinning in the plagioclase grains is abundant. In some samples, tabular plagioclase grains are rimmed by anorthoclase (Fig. 3b). Micrographic intergrowths of quartz±orthoclase±albite and discrete grains of these minerals fill interstices (Fig. 3a, 3b, 3c). Fe-Ti oxides (Fig. 3e) are represented by elongated grains of ilmenite, with or without rare Ti-magnetite lamellae (Fig. 3f), and isometric grains of Ti-magnetite with numerous ilmenite lamellae (forming three systems) (Fig. 3g). Ti-magnetite is preserved as unique relicts and generally is completely replaced by titanite; the ilmenite lamellae therein seem to be much more resistant to the metamorphic replacement. Fe-Ti oxides contain inclusions of silicate minerals as, for example, shown in Fig. 3h.

Gabbroic diorites exhibit mineral assemblages and textures typical of gabbro and Fe-Ti gabbro and differ from the latter only in modal mineral abundances (chiefly elevated quartz, biotite and potassium feldspar abundances). As the gabbro and Fe-Ti gabbro, gabbroic diorites are massive fine-

to medium-grained mesocratic hypidiomorphic-granular and granophyric rocks. Their peculiar feature is the wide occurrence of micrographic intergrowths of quartz, orthoclase and albite.

Metamorphic replacement of minerals is recorded by partial to complete replacement of primary pyroxenes and hornblende by greenish actinolite and chlorite. Core plagioclases are commonly substituted by calcium-potassium-sodium zeolites. In some samples, plagioclases are totally replaced by albite or albite-oligoclase, prehnite, epidote and pumpellyite; no primary zonation was preserved in these samples. Biotite is substituted mainly by chlorite, Ti-magnetite and ilmenite by titanite. In some well-metamorphosed samples, a secondary biotite forming sharp euhedral plates and associated with chlorite and albite has formed. Traces of metamorphic calcite, stilpnomelane and muscovite also occur. A few rocks, which are completely metamorphosed, exhibit no primary magmatic textures (Fig. 3d), and relict primary minerals therein are represented by quartz, apatite and ilmenite only.

Composition of minerals

Major elements in minerals were analyzed in polished thin sections using a Cameca-SX100 electron microprobe at the V.I. Vernadsky Institute of Geochemistry and Analytical Chemistry (GEOKHI RAS) at 15kV accelerating voltage and 30 nA beam current. The diameter of the beam was 5 µm for plagioclase to predict Na loss and 1-2µm for all other minerals analyzed. Counting time was 20/10 s (peak/background). Natural standards from the Smithsonian Institution were used. The analytical accuracy for silicate minerals was monitored by regular measurements of the Cr-augite. The single point analytical errors were ±2% rel. for major components (10-100 wt %), ±5% rel. for minor components (2-10 wt %), ±10% rel. for components accounting for 1-2 wt %, and ±20 % rel. for components accounting for less than 1 wt %.

Major-element variations in minerals of the Anyui province rocks

Compositions of primary minerals are shown in Table 3. In most of the samples studied, augites have relatively high to moderate magnesium-numbers

Table 3. Primary mineral compositions.

N	1	2	3	4	5	6	7	8	9	10
Sample	KE9-71	KE9-71	KE9-71	KE9-71	KE9-71	KE9-71	KE9-71	KE9-72	KE9-72	KE9-72
Mineral	Cpx-C	Cpx-R	Bi	P11	P12/Qtz	Ilm	Ti-Mag	Cpx	Hbl	Ilm-Lam
Points	2	2	2	2	1	4	1	3	2	1
SiO ₂	50.65	50.89	35.38	55.07	65.94	0.05	0.23	50.99	47.01	0.14
TiO ₂	0.91	0.72	3.42	0.06	0.00	47.45	6.15	0.64	0.99	50.62
Al ₂ O ₃	1.70	1.56	12.37	27.90	21.64	0.06	0.87	1.38	5.33	0.03
FeO	14.05	13.31	27.66	0.48	0.22	49.37	84.49	13.62	20.64	45.45
MnO	0.42	0.41	0.08	0.00	0.00	0.96	0.00	0.46	0.36	1.45
MgO	13.68	12.36	7.06	0.06	0.01	0.08	0.02	11.77	10.42	0.06
CaO	17.29	19.52	0.04	10.41	2.92	0.03	0.36	20.21	10.25	0.59
Na ₂ O	0.26	0.26	0.09	5.28	9.48	0.00	0.05	0.24	1.74	0.03
K ₂ O	0.01	0.00	8.46	0.42	0.30	0.01	0.01	0.00	0.71	0.00
Cr ₂ O ₃	0.00	0.01	0.03	0.02	0.00	0.03	0.05	0.04	0.00	0.04
NiO						0.01				
V ₂ O ₃						0.66	1.77			
Sum	98.96	99.04	94.59	99.69	100.51	98.72	94.01	99.36	97.46	98.40
Cl										
Mg#	63.4	62.4	31.3					60.6	47.4	
xAn				50.9	14.3					

Table 3. (continued).

N	11	12	13	14	15	16	17	18	19	20
Sample	KE9-72L	KE9-73	KE9-73	KE9-73	KE9-73	KE9-73	KE9-73	KE9-73	KE9-73	KE9-73
Mineral	Ilm	Cpx	Pig	Hbl	Bi	P11	P12/Qtz	Ort/Sim Qtz	Ilm	Ti-Mag1
Points	1	3	3	2	2	2	2	2	2	2
SiO ₂	0.31	50.37	51.58	47.02	35.88	54.60	59.97	64.28	0.04	0.13
TiO ₂	50.72	0.94	0.27	1.38	3.90	0.09	0.04	0.00	47.19	12.70
Al ₂ O ₃	0.08	2.02	0.40	5.64	12.87	29.15	25.64	19.38	0.05	1.80
FeO	45.06	13.96	28.84	18.21	26.06	0.59	0.56	0.06	47.94	78.17
MnO	1.44	0.39	0.69	0.22	0.08	0.01	0.03	0.02	0.96	0.30
MgO	0.12	12.60	14.80	11.60	9.33	0.06	0.03	0.02	0.09	0.04
CaO	0.22	18.55	3.42	10.66	0.16	11.52	7.09	0.05	0.01	0.05
Na ₂ O	0.01	0.26	0.07	1.66	0.05	4.69	6.87	0.29	0.03	0.04
K ₂ O	0.01	0.01	0.01	0.73	6.66	0.32	0.72	16.28	0.01	0.00
Cr ₂ O ₃	0.03	0.02	0.02	0.02	0.00	0.00	0.01	0.00	0.03	0.07
NiO									0.00	
V ₂ O ₃									0.66	2.21
Sum	97.99	99.11	100.10	97.13	95.00	101.03	100.96	100.38	97.01	95.51
Cl										
Mg#		61.7	47.8	53.2	39.0					
xAn						56.5	34.8			

Table 3. (continued).

N	21	22	23	24	25	26	27	28	29	30
Sample	KE9-73	GY9-76	GY9-76	GY9-78	GY9-78	GY9-78	GY9-82a	GY9-82a	GY9-82a	GY9-82a
Mineral	Ti-Mag2	Hbl	Ilm	Hbl	Ap	Ilm	Hbl	Pl-C	Pl-R	Ort
Points	1	2	2	2	1	1	2	2	3	1
SiO ₂	0.12	45.14	0.04	43.63	0.19	0.04	45.93	57.61	63.51	64.79
TiO ₂	5.80	1.47	53.11	1.61	0.03	51.36	1.30	0.06	0.00	0.02
Al ₂ O ₃	2.15	5.81	0.03	6.63	0.00	0.03	5.81	27.21	24.06	18.86
FeO	85.75	22.40	43.27	26.56	0.77	45.88	20.93	0.44	0.40	0.48
MnO	0.16	0.29	2.40	0.37	0.07	1.58	0.30	0.03	0.01	0.03
MgO	0.07	8.14	0.07	5.81	0.01	0.05	9.96	0.01	0.03	0.04
CaO	0.02	10.41	0.04	10.13	53.80	0.06	10.07	8.87	4.51	0.01
Na ₂ O	0.00	1.47	0.02	1.46	0.00	0.00	1.65	5.67	8.07	0.25
K ₂ O	0.01	0.70	0.00	0.99	0.00	0.00	0.82	0.57	0.67	16.19
Cr ₂ O ₃	0.06	0.04	0.00	0.02	0.06	0.04	0.04	0.04	0.02	0.00
NiO										
V ₂ O ₃	1.89									
Sum	96.03	95.88	98.97	97.21	54.93	99.04	96.81	100.51	101.30	100.66
Cl										
Mg#		39.3		28.1			45.9			
xAn								44.8	22.7	

Table 3. (continued).

N	31	32	33	34	35	36	37	38	39	40
Sample	GY9-82b	GY9-82b	GY9-82b	GY9-82b	GY9-82b	GY9-85	GY9-85	GY9-85	GY9-85	GY9-87
Mineral	Hbl	Bi	Pl-C	Pl-R	Ort	Hbl	Bi	Ort	Ilm	Cpx
Points	3	2	2	1	1	4	3	2	1	2
SiO ₂	44.58	33.30	58.62	64.65	66.47	43.71	31.99	63.86	0.04	49.60
TiO ₂	1.33	3.57	0.02	0.00	0.01	1.38	2.58	0.03	53.11	0.60
Al ₂ O ₃	6.47	12.73	25.63	22.02	19.65	6.11	12.51	19.63	0.02	1.14
FeO	24.59	30.91	0.39	0.04	0.07	26.70	35.58	0.27	46.15	19.19
MnO	0.24	0.18	0.01	0.00	0.00	0.38	0.20	0.00	1.82	0.70
MgO	7.17	5.84	0.02	0.01	0.00	5.62	3.52	0.02	0.03	7.44
CaO	10.42	0.21	7.49	2.92	0.00	10.05	0.36	0.08	0.01	20.33
Na ₂ O	1.45	0.10	5.93	8.93	0.26	1.97	0.04	0.27	0.01	0.24
K ₂ O	0.87	6.51	0.64	0.69	14.94	0.88	5.25	14.44	0.00	0.00
Cr ₂ O ₃	0.02	0.03	0.00	0.00	0.00	0.01	0.02	0.00	0.00	0.00
NiO										
V ₂ O ₃										
Sum	97.14	93.38	98.76	99.27	101.40	96.82	92.04	98.61	101.18	99.24
Cl										
Mg#	34.2	25.2				27.3	15.0			40.9
xAn			39.4	14.7						

Table 3. (continued).

N	41	42	43	44	45	46	47	48	49	50
Sample	GY9-87	GY9-87	GY9-87	PS9-89						
Mineral	Hbl	Ort	Ilm	Cpx1	Cpx2	Hbl	Bi	Pl-C	Pl-R	Ano
Points	4	2	2	2	2	2	2	2	1	2
SiO ₂	44.64	66.19	0.06	48.03	50.52	42.68	34.95	54.76	59.13	64.49
TiO ₂	1.50	0.02	49.48	0.98	1.04	1.78	4.01	0.06	0.03	0.02
Al ₂ O ₃	6.20	19.43	0.04	3.63	1.96	7.20	12.07	28.00	25.33	19.06
FeO	25.59	0.10	47.64	13.12	12.02	25.96	28.68	0.58	0.36	0.11
MnO	0.33	0.00	2.35	0.27	0.34	0.23	0.13	0.02	0.01	0.00
MgO	7.00	0.00	0.03	12.92	12.84	5.69	5.77	0.10	0.02	0.02
CaO	10.15	0.02	0.08	18.02	19.82	10.37	0.16	10.68	7.17	0.33
Na ₂ O	2.01	0.25	0.00	0.28	0.28	1.66	0.15	5.04	6.58	3.31
K ₂ O	0.91	14.89	0.03	0.02	0.01	0.97	7.92	0.39	0.84	11.13
Cr ₂ O ₃	0.00	0.00	0.03	0.00	0.04	0.01	0.03	0.00	0.02	0.01
NiO										
V ₂ O ₃			0.89							
Sum	98.35	100.89	100.63	97.27	98.86	96.57	93.87	99.63	99.49	98.48
Cl										
Mg#	32.8			63.7	65.6	28.1	26.4			
xAn								52.7	35.7	

Table 3. (continued).

N	51	52	53	54	55	56	57	58	59	60
Sample	PS9-89	PS9-89	PS9-89	PS9-92	PS9-92	PS9-92	PS9-92	PS9-92	PS9-92	GY9-98
Mineral	Ort/Sim Qtz	Ort	Ilm	Cpx	Hbl-C	Hbl- R/Qtz	Bi	Pl/Ilm	Ort	Ilm
Points	1	1	2	2	2	2	3	1	1	1
SiO ₂	65.90	63.08	0.03	50.32	45.53	45.50	35.39	54.29	64.16	0.06
TiO ₂	0.02	0.02	48.47	1.20	1.07	1.39	4.55	0.14	0.00	55.03
Al ₂ O ₃	19.12	18.66	0.07	3.02	5.68	5.91	12.70	28.14	18.64	0.00
FeO	0.14	0.66	46.76	11.09	22.34	25.09	27.96	0.88	0.07	44.47
MnO	0.00	0.00	1.85	0.21	0.27	0.24	0.11	0.01	0.00	2.22
MgO	0.03	0.01	0.07	13.43	9.15	7.11	6.26	0.02	0.01	0.07
CaO	0.19	0.00	0.02	19.78	10.08	10.19	0.01	10.71	0.01	0.00
Na ₂ O	2.98	0.20	0.00	0.30	1.77	1.52	0.22	4.79	0.22	0.04
K ₂ O	12.14	15.50	0.00	0.01	0.83	0.64	7.97	0.40	15.84	0.00
Cr ₂ O ₃	0.00	0.02	0.00	0.05	0.03	0.04	0.06	0.04	0.01	0.05
NiO			0.02							
V ₂ O ₃			0.58							
Sum	100.53	98.15	97.88	99.41	96.73	97.64	95.23	99.42	98.96	101.93
Cl										
Mg#				68.3	42.2	33.6	28.5			
xAn								53.9		

Table 3. (continued).

N	61	62	63	64	65	66	67	68	69	70
Sample	GY9-99	GY9-99	GY9-99	GY9-99	GY9-101	GY9-101	P-11-7	P-11-7	P-11-7	P-11-7
Mineral	Hbl1	Hbl2	Bi	Ilm	Hbl	Ilm	Cpx-C	Cpx-R	Hbl1	Hbl2
Points	2	2	2	3	2	2	2	4	1	3
SiO ₂	48.05	46.85	37.52	0.05	45.73	0.08	52.14	51.57	46.81	44.13
TiO ₂	1.07	1.16	1.93	51.87	1.53	50.69	0.65	0.85	1.46	1.40
Al ₂ O ₃	4.97	5.74	12.66	0.03	6.95	0.02	2.15	2.09	6.15	5.62
FeO	19.09	20.19	25.55	45.08	21.02	43.23	10.19	12.75	16.42	25.38
MnO	0.25	0.21	0.15	2.41	0.26	2.99	0.28	0.34	0.24	0.36
MgO	10.87	9.60	8.41	0.10	8.74	0.10	14.35	14.26	12.71	7.15
CaO	10.50	10.74	0.03	0.05	10.70	0.05	19.73	17.81	10.25	9.45
Na ₂ O	1.10	1.18	0.03	0.00	1.18	0.02	0.30	0.27	2.19	1.94
K ₂ O	0.52	0.67	9.02	0.01	0.85	0.01	0.01	0.01	0.67	0.77
Cr ₂ O ₃	0.01	0.01	0.05	0.01	0.02	0.47	0.02	0.00	0.01	0.00
NiO		0.07		0.01		0.01				
V ₂ O ₃		0.08		0.53		0.63				
Sum	96.42	96.50	95.36	100.14	96.96	98.27	99.81	99.94	96.90	96.21
Cl									0.10	0.40
Mg#	50.4	45.9	37.0		42.6		71.5	66.6	58.0	33.4
xAn										

Table 3. (continued).

N	71	72	73	74	75	76	77	78	79	80
Sample	P-11-7	P-11-7	P-11-7	P-11-7a	P-11-7a	P-11-7a	P-11-7a	P-11-7a	P-11-7a	P-11-7a
Mineral	Pl	Ilm	Ap	Cpx-C	Cpx-R	Hbl-C	Hbl-R/Qtz	Pl1/Cpx	Pl2	Pl3
Points	2	2	1	2	2	2	2	2	2	2
SiO ₂	58.82	0.53	0.75	50.57	51.57	46.98	44.89	51.11	53.61	58.41
TiO ₂	0.02	52.11	0.02	0.92	0.64	1.14	1.30	0.04	0.08	0.05
Al ₂ O ₃	25.49	0.13	0.24	3.50	2.22	4.54	5.36	30.06	28.52	26.38
FeO	0.43	44.85	1.22	8.89	8.41	22.52	25.73	0.79	1.02	0.79
MnO	0.00	2.19	0.06	0.27	0.27	0.40	0.32	0.01	0.01	0.02
MgO	0.06	0.08	0.14	15.51	15.84	8.98	6.69	0.15	0.22	0.16
CaO	6.88	0.52	52.74	19.08	19.31	10.26	9.44	13.87	10.50	6.83
Na ₂ O	6.98	0.02	0.04	0.31	0.25	1.71	1.73	3.67	4.59	6.43
K ₂ O	0.69	0.01	0.01	0.00	0.00	0.67	0.62	0.17	0.72	0.89
Cr ₂ O ₃	0.00	0.01	0.03	0.14	0.08	0.00	0.02	0.00	0.02	0.03
NiO										
V ₂ O ₃										
Sum	99.38	100.46	55.25	99.18	98.58	97.20	96.10	99.86	99.28	99.99
Cl			0.06			0.22	0.39			
Mg#				75.7	77.1	41.6	31.7			
xAn	33.8							67.0	53.4	35.0

Table 3. (continued).

N	81	82	83	84	85	86	87	88	89	90
Sample	P-11-7a	P-11-7a	T-05-5							
Mineral	PI4-R/Qtz	Ilm	Cpx1	Cpx2	Pig	Opx	Bi-C	Bi-R	Pl1/Cp	Pl2/Qtz
Points	2	2	3	2	3	2	3	2	3	2
SiO ₂	65.15	0.11	49.86	50.85	50.57	49.62	35.94	34.28	54.69	59.49
TiO ₂	0.03	50.60	0.91	0.67	0.42	0.34	4.49	3.24	0.08	0.02
Al ₂ O ₃	22.08	0.07	1.90	1.31	0.69	0.32	12.60	12.85	28.48	25.51
FeO	0.41	45.87	15.64	15.61	26.61	33.00	22.89	28.29	0.67	0.34
MnO	0.02	2.06	0.39	0.48	0.74	0.91	0.09	0.14	0.00	0.03
MgO	0.03	0.10	12.46	12.22	15.24	12.65	9.30	6.67	0.07	0.03
CaO	2.22	0.17	16.96	17.99	4.74	2.64	0.05	0.11	10.92	7.18
Na ₂ O	9.02	0.03	0.26	0.26	0.10	0.06	0.23	0.05	5.22	7.14
K ₂ O	0.57	0.00	0.01	0.02	0.00	0.01	8.62	7.96	0.26	0.65
Cr ₂ O ₃	0.01	0.00	0.02	0.02	0.00	0.01	0.01	0.07	0.00	0.01
NiO										
V ₂ O ₃										
Sum	99.53	99.01	98.41	99.44	99.13	99.54	94.22	93.66	100.40	100.40
Cl							0.34	0.33		
Mg#			58.7	58.2	50.5	40.6	42.0	29.6		
xAn	11.6								52.8	34.4

Table 3. (continued).

N	91	92	93
Sample	T-05-5	T-05-5	T-05-5
Mineral	Ort	Ilm	Ti-Mag
Points	2	2	2
SiO ₂	64.24	0.07	0.10
TiO ₂	0.00	48.69	16.22
Al ₂ O ₃	18.47	0.03	1.49
FeO	1.17	46.98	74.78
MnO	0.05	1.72	0.62
MgO	0.18	0.03	0.02
CaO	0.10	0.04	0.02
Na ₂ O	0.59	0.02	0.00
K ₂ O	14.44	0.00	0.00
Cr ₂ O ₃	0.08	0.16	0.03
NiO			
V ₂ O ₃			
Sum	99.30	97.75	93.29
Cl			
Mg#			
xAn			

Notes: C – core, R – rim, numbers correspond to different mineral generations. min/min – phases at a contact. Sim – micrographic intergrowths. For other acronyms see caption to Figure 3.

(note: $mg\# = 100 * Mg / (Mg + Fe_{tot})$) was similarly calculated for all minerals and whole rocks) of 58-77 that drop as low as 41 in the gabbroic diorite (Fig. 4) with the lowest magnesium number of rock (sample GY9-87). The $mg\#$ variations of augite within a single sample commonly are negligible but in most samples outer parts of augite grains are fully replaced. Only two samples (KE9-71, P11-7) contain augite that exhibits core-to-rim zoning. All augites are relatively low in titanium (0.6-1.04 wt. %, TiO_2) and sodium (0.24-0.30 wt. %, Na_2O); concentrations of these elements remain nearly constant in the whole range of augite magnesium number variations.

Primary **hornblendes**, edenites and ferroedenites (Leake, et al., 1997), have moderate to low magnesium-numbers of 27.3-58.0 (Fig. 5) that do not cover the range of magnesium number variations in clinopyroxenes. Hornblendes generally show moderately low aluminum (4.54-7.20 wt. %, Al_2O_3), elevated titanium (0.99-1.78 wt. %, TiO_2) contents

and are rich in potassium (0.52-0.97 wt. %, K_2O). Some samples studied (GY9-92, GY9-99, P-11-7, P-11-7a) contain hornblendes of widely variable magnesium-numbers.

Biotite exhibits wide variations in FeO^{tot}/MgO ratio chiefly ranging in the interval of 2.5-5.3 and reaching 10.1 in the gabbroic diorite (sample GY9-85), i.e. biotites become richer in siderophyllite and annite components. Al_2O_3 abundances of 12.07-12.87 wt. % remain nearly constant. TiO_2 content decreases slightly as the $mg\#$ of biotite decreases. They are relatively high (2.6-4.6 wt. %, TiO_2) excluding sample GY9-99 in which somewhat lowered titanium content can be related to partial recrystallization of the biotite. In some samples biotites reveal lowered K_2O contents that can be a result of partial metamorphic recrystallization or replacement of this mineral.

Plagioclases are represented by both igneous and metamorphic (albite) generations. Primary

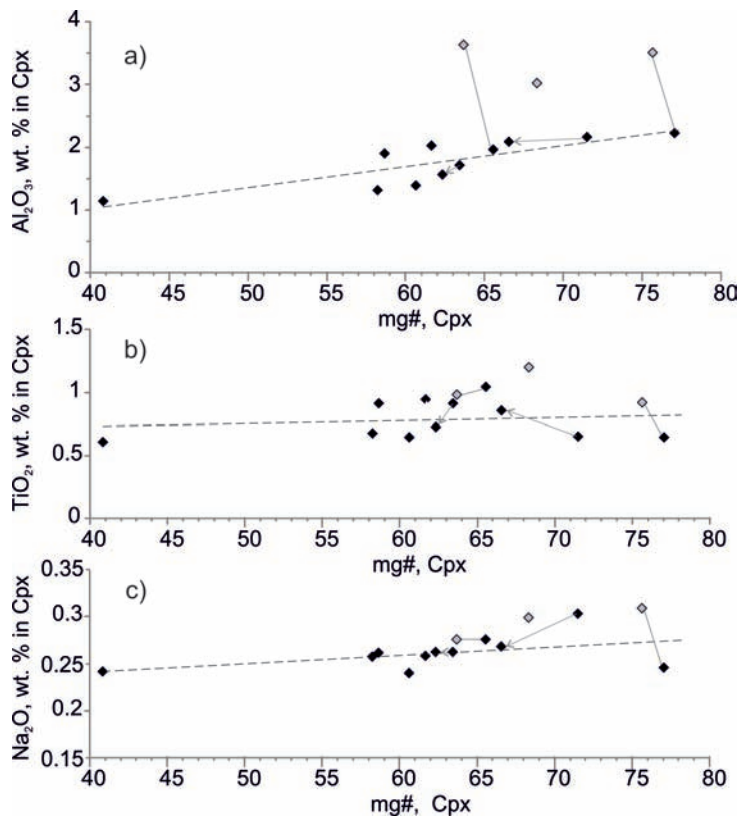


Fig. 4. Oxide, wt. % vs. $mg\#$, Cpx plot. Black and grey diamonds are for low-Al and medium-Al clinopyroxenes in the Anyui province sills, correspondingly. Grey arrows show core-to-rim zoning in the sample; grey lines connect coexisting augite generations (measured in different grains) in the sample. Individual data points characterize individual samples (in this and other diagrams for minerals).

plagioclases have appreciable admixtures of iron (0.2-0.8 wt. %, FeO) and K_2O (0.2-0.9 wt. %) and display a clear regularity in decreasing iron contents and increasing potassium contents with decreasing xAn (note: $xAn = 100 * Ca / (Ca + Na + K)$) in plagioclase. As mentioned above, primary plagioclases are zoned. In gabbro, their cores are composed of labradorite (xAn67-51) that gradually ranges into andesine (xAn36-34) rims. At the contact with quartz, rim plagioclases become sodic oligoclase (xAn14-12). In one of the samples studied (P-11-7a), they cover the whole range of compositions from labradorite xAn72 to oligoclase xAn12. Most calcium plagioclases are confined to core grains embedded in clinopyroxenes. In the gabbroic diorite, tabular feldspar grains are made of andesine (xAn45-39) cores and oligoclase (xAn23-14) rims. Therefore, in all samples studied plagioclases reveal wide compositional variations.

Alkali feldspars are represented by anorthoclase and orthoclase. Anorthoclase was measured only in one sample (PS9-89) in which it constitutes the outermost rim of the zoned tabular feldspar (Fig. 3c). In this sample, orthoclase intergrown with quartz in interstices is sodium-bearing variety (3 wt. % Na_2O) that seems to have primary magmatic composition.

In this and other (more intensively metamorphosed) samples studied, pure orthoclase; however, occurs along with sodium orthoclase in micrographyc structures. In all samples albitic plagioclase seems to have a metamorphic origin. We suppose that pure orthoclase and albite in micrographyc structures are products of metamorphic recrystallization of primary magmatic sodium orthoclase (and probably also anorthoclase) and primary magmatic plagioclase (probably sodium oligoclase or albite), respectively.

Ti-magnetites were measured only in three samples and are characterized by variable TiO_2 content of 6.15-16.22 even within a single sample. This is probably related to different degrees of the magnetite to ilmenite exsolution in different points of analyses. All Ti-magnetites demonstrate high V_2O_3 contents (1.8-2.2 wt. %), elevated Al_2O_3 contents (0.9-2.2 wt. %) and relatively low MnO contents (up to 0.6 wt. %).

Ilmenites show slight $TiO_2 - FeO_{total}$ variations with ilmenite composing grains and lamellae in Ti-magnetite in a single sample having similar compositions. The only significant admixture in ilmenites is MnO (0.96-2.40 wt. %).

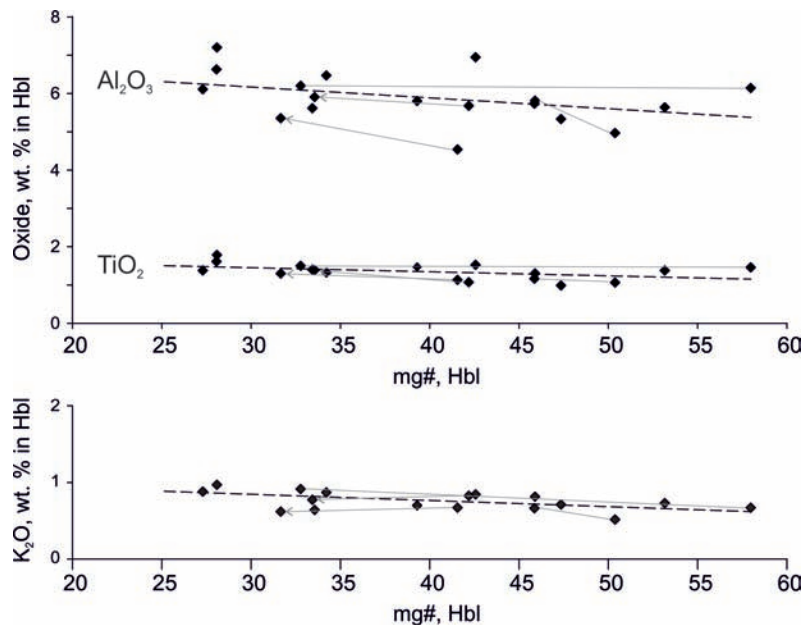


Fig. 5. Oxide, wt. % vs. mg#, Hbl plots. Grey arrows show a core-to-rim zoning; grey lines connect compositions of minerals coexisting in one sample.

BULK ROCK MAJOR AND TRACE-ELEMENT COMPOSITIONS

Major and trace elements in bulk rocks were measured at the GEOKHI RAS, Moscow, Russia. Samples were carefully cleaned before crushing but not leached. Rocks (~300-400 g) were crushed and powdered (~30-40 g) using a jaw crushing and vibrating cup mill. The major elements were determined by the XRF method with a Phillips PW-1600 equipment. The calibration was performed using international (Govindaraju, 1994) and domestic rock standards as well as internal standards. The trace-element abundances were determined by Inductively Coupled Plasma Mass Spectrometry with a Finnigan Element XR instrument. Sample

preparation was done in a microwave oven using the method of bulk rock acid digestion. The precision and accuracy of analyses were controlled by regular measurements of international (BCR-2) and internal rock standards. Detection limits were 0.01 ng/g for heavy and medium elements and 0.1 ng/g for light elements. Analytical error was 1-3% rel. (one standard deviation). Element contents were calculated using standard solutions ICP-MS-68A, HPS (A and B) with known element concentrations.

Principle features of bulk rock compositions

Bulk rock compositions are given in Table 4. In the TAS diagram (Fig. 6a) the plutonic rock samples investigated fall into the field of gabbro and gabbroic

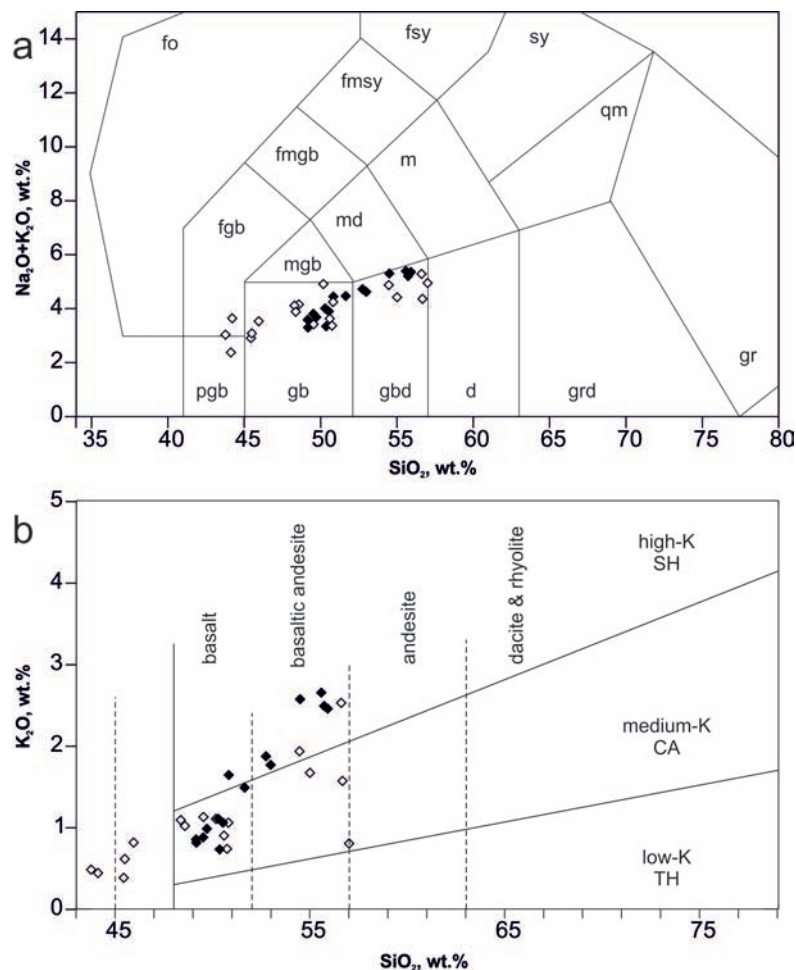


Fig. 6. Nomenclature of the rocks studied (open diamonds) and calculated melts (filled diamonds).

(a) TAS (total alkali, wt. % vs. SiO₂, wt. %) diagram adopted for plutonic rocks (Middlemost, 1994). Acronyms are as follows: pgb – peridotgabbro; gb – gabbro; gbd – gabbroic diorite; d – diorite; grd – granodiorite; gr – granite; mgb – monzogabbro; md – monzodiorites; m – monzonite; qm – quartz monzonite; sy – syenite; fgb – foid gabbro; fmgb – foid monzogabbro; fmsy – foid monzosyenite; fsy – foid syenite; fo – foidotite.

(b) SiO₂, wt. % vs. K₂O, wt. % diagram for volcanic rocks (LeMaitre et al., 1989) demonstrating series affinity of the melts calculated; actual rock compositions are shown for comparison.

Table 4. Bulk rock major and trace element compositions

	1	2	3	4	5	6	7	8	9
Sample	GY9-101	PS9-92	GY9-74	GY9-79	KE9-71	PS9-89	KE9-73	GY9-99	GY9-81
SiO ₂	49.25	48.59	42.55	43.94	45.03	47.21	44.61	42.08	46.83
TiO ₂	2.35	2.58	6.17	5.28	5.72	3.82	5.98	3.59	4.62
Al ₂ O ₃	13.38	13.77	11.34	11.53	12.87	12.69	12.49	10.43	11.87
FeO	12.79	13.31	18.33	16.82	16.43	15.77	17.11	21.53	17.55
MnO	0.171	0.168	0.214	0.208	0.222	0.203	0.229	0.221	0.215
MgO	6.00	4.66	6.14	6.13	5.12	4.90	5.13	8.36	3.75
CaO	9.50	8.64	9.26	9.70	8.82	8.18	9.13	6.52	7.74
Na ₂ O	2.55	3.68	2.48	2.44	2.66	3.05	2.42	1.84	2.70
K ₂ O	0.72	1.07	0.47	0.38	0.80	0.99	0.61	0.43	1.06
Cr ₂ O ₃	0.018	0.011	0.000	0.000	0.000	0.001	0.000	0.014	0.000
P ₂ O ₅	0.312	0.345	0.250	0.274	0.317	0.362	0.347	0.356	0.468
LOI	1.92	2.16	1.41	2.04	0.85	1.49	0.62	2.94	1.78
Sum	98.96	99.00	98.61	98.74	98.85	98.67	98.68	98.30	98.58
Rb	16	33	10	9	26	35	20	18	40
Ba	290	259	164	116	239	392	201	121	344
Th	2.14	2.83	1.71	1.92	2.01	2.74	2.03	2.90	3.14
U	0.68	0.78	0.56	0.62	0.67	0.88	0.70	0.79	0.97
Nb	14.7	16.2	17.8	17.2	20.4	18.9	20.9	22.5	27.6
Ta	0.66	0.77	1.19	1.00	1.12	1.09	1.07	1.21	1.44
La	18.5	22.0	15.4	16.5	18.3	21.2	18.1	26.7	28.9
Ce	43	51	37	39	44	50	43	64	68
Pb	5.84	2.11	4.09	4.31	3.84	2.80	2.98	1.31	8.33
Pr	5.8	6.7	4.9	5.3	5.9	6.6	5.8	8.3	8.9
Sr	306	172	245	291	249	316	224	72	338
Nd	27	30	23	25	28	31	27	38	41
Sm	6.5	7.4	5.9	6.3	7.0	7.5	6.8	9.3	9.8
Zr	116	91	139	117	207	179	209	126	248
Hf	3.2	2.8	3.8	3.7	5.5	5.0	5.4	3.6	6.5
Eu	2.09	2.22	1.94	1.92	2.20	2.30	2.20	2.19	3.08
Gd	7.3	8.1	6.6	7.0	7.8	8.3	7.6	10.1	11.0
Tb	1.25	1.39	1.16	1.22	1.37	1.45	1.33	1.71	1.87
Dy	7.3	8.1	7.0	7.3	8.1	8.5	7.9	10.1	11.1
Y	42	47	41	42	48	50	46	58	65
Ho	1.47	1.62	1.41	1.45	1.67	1.73	1.61	2.00	2.22
Er	4.3	4.8	4.1	4.2	4.9	5.0	4.7	5.8	6.5
Tm	0.58	0.65	0.56	0.58	0.68	0.69	0.66	0.77	0.89
Yb	3.7	4.2	3.8	3.5	4.5	4.6	4.3	4.8	5.9
Lu	0.50	0.60	0.49	0.46	0.67	0.66	0.63	0.65	0.84
V	396	391	833	754	658	618	727	495	416
Cr	235	209	11	14	13	61	16	233	14
Co	34	38	54	48	50	44	60	76	43
Ni	80	98	25	47	30	68	11	223	29
Cu	57	65	305	302	343	278	44	271	61
Zn	110	105	135	128	143	147	145	195	178

Table 4. (continued).

	10	11	12	13	14	15	16	17
Sample	GY9-102	PS9-90	GY9-76	GY9-82a	GY9-78	GY9-82b	GY9-87	GY9-84
SiO ₂	47.53	49.03	49.29	52.76	55.56	54.89	54.81	54.18
TiO ₂	3.38	3.24	4.31	2.91	2.56	2.63	2.26	2.55
Al ₂ O ₃	12.28	12.41	10.63	12.62	12.20	11.64	10.98	11.52
FeO	16.33	15.69	17.27	15.47	13.47	14.62	15.77	16.20
MnO	0.204	0.185	0.266	0.171	0.137	0.142	0.202	0.190
MgO	5.87	4.20	3.74	3.18	2.52	2.23	2.20	2.42
CaO	6.58	7.06	7.79	4.42	5.43	4.91	5.41	6.22
Na ₂ O	2.20	3.07	2.65	2.85	4.04	2.67	2.70	2.71
K ₂ O	1.09	1.03	0.88	1.88	0.79	2.46	1.52	1.65
Cr ₂ O ₃	0.006	0.005	0.000	0.002	0.000	0.000	0.000	0.001
P ₂ O ₅	0.481	0.551	0.584	0.601	0.744	0.773	0.857	0.856
LOI	2.72	2.17	1.20	1.73	1.43	1.64	1.80	0.00
Sum	98.66	98.64	98.61	98.60	98.88	98.61	98.51	98.50
Rb	50	34	38	63	28	61	45	40
Ba	377	624	250	799	196	853	438	572
Th	3.28	3.66	3.71	4.78	5.72	7.20	5.91	5.67
U	0.95	1.08	1.07	1.09	1.31	2.95	1.45	1.58
Nb	23.5	23.5	32.2	32.8	38.1	35.3	40.2	38.5
Ta	1.12	1.12	1.70	1.67	1.97	1.58	2.14	1.86
La	30.1	33.7	33.9	39.3	54.2	54.8	55.2	53.2
Ce	71	79	82	94	126	130	131	128
Pb	6.50	3.69	5.61	3.07	1.50	2.83	5.40	2.60
Pr	9.1	10.1	10.8	11.8	16.2	16.1	16.7	16.1
Sr	257	300	244	273	97	192	129	124
Nd	42	45	50	53	72	72	75	73
Sm	9.9	10.6	11.9	12.4	16.9	16.6	17.6	17.1
Zr	111	69	175	93	180	303	163	283
Hf	3.2	2.3	4.6	3.5	4.9	8.2	4.8	7.3
Eu	2.92	2.75	3.36	3.47	4.02	3.76	4.08	4.17
Gd	11.2	11.6	13.2	13.5	18.3	17.9	19.3	18.7
Tb	1.86	1.94	2.24	2.24	3.07	3.00	3.23	3.12
Dy	10.8	11.2	13.2	13.1	17.7	17.3	18.7	18.0
Y	64	66	78	78	104	104	110	108
Ho	2.14	2.24	2.62	2.61	3.53	3.45	3.71	3.58
Er	6.2	6.6	7.6	7.6	10.1	10.3	10.9	10.5
Tm	0.82	0.89	1.02	1.04	1.35	1.39	1.44	1.40
Yb	5.2	5.9	6.5	6.8	8.5	9.1	9.4	9.1
Lu	0.69	0.85	0.91	0.97	1.15	1.31	1.35	1.30
V	491	417	197	227	136	126	46	96
Cr	94	83	16	56	38	43	23	33
Co	44	40	35	31	26	31	23	27
Ni	60	51	7	40	23	38	34	35
Cu	169	112	19	56	6	7	16	26
Zn	239	128	200	111	66	107	217	171

diorite. All rock varieties follow a trend of simultaneous increase of silica and total alkali elements and belong to a moderate alkaline series. In binary diagrams (Fig. 7) gabbro and gabbroic diorite of the Anyui province of eastern Chukotka form linear and gently curved trends. The mg# of rock samples range from 19.4 to 38.1 and decreases from gabbro to gabbroic diorite. As mg# of gabbro and gabbroic diorite decreases, contents of Al_2O_3 and CaO decrease, concentrations of P_2O_5 increase and abundances of TiO_2 remain nearly constant. In contrast, Fe-Ti gabbro exhibit irregular variations and lie out of the trends in the plots for Al_2O_3 and TiO_2 .

In multi-element diagrams (Fig. 8), the gabbro, Fe-Ti gabbro and gabbroic diorite show spectra, which are principally similar in shape. The spectra reveal a relative enrichment of all investigated rocks

in more incompatible lithophile elements (such as Th, U, light REE) relative to less incompatible ones (such as Y and heavy REE). Contents of lithophile elements gradually increase from gabbro to gabbroic diorite; the Fe-Ti gabbro has trace-element contents similar to that of the gabbro or intermediate between the gabbro and gabbroic diorite. The rocks exhibit negative anomalies of Nb-Ta, Zr-Hf, Sr and P. The anomalies of Zr-Hf are very small or almost negligible in some samples of Fe-Ti gabbro and gabbroic diorite. A titanium anomaly is negligible in gabbro; it becomes positive in some Fe-Ti gabbro and negative in gabbroic diorite.

BULK ROCK SM-ND ISOTOPE COMPOSITIONS

Neodymium and strontium isotopic measure-

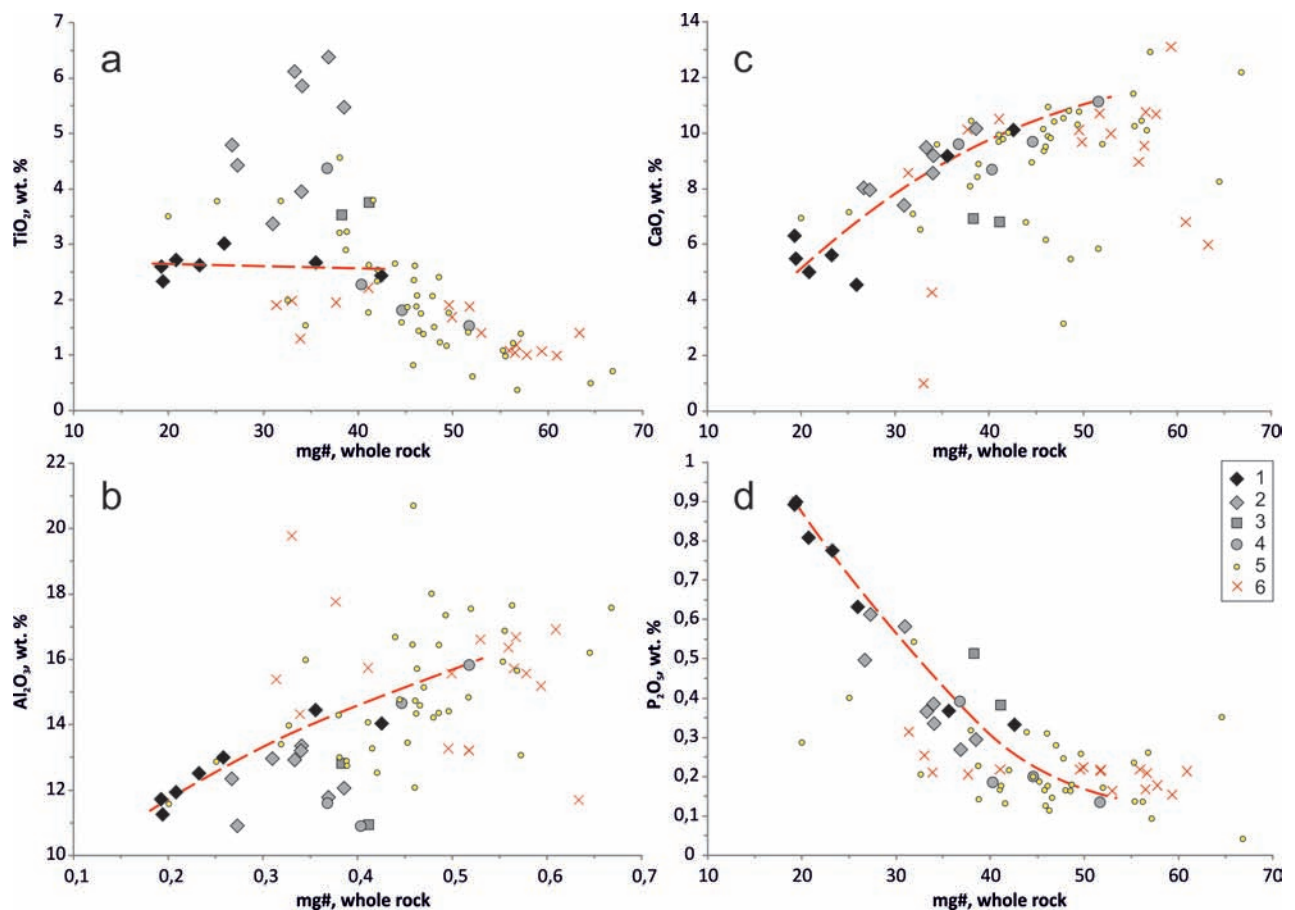


Fig. 7. Mg#, whole rock vs. oxide, wt. % diagrams. The original data are compared with those published on the Bilibino and Cape Schmidt areas (Gel'man, 1963; Degtyaryov, 1975) and the New Siberian Islands (Kuz'michov and Pease, 2007). Symbols 1 to 5 are for the Anyui province of Chukotka: gabbro and gabbroic diorite studied (1); Fe-Ti gabbro studied (2); investigated Fe-Ti gabbro with significant admixture of silicate phases or strongly allochemically metamorphosed (3); gabbroic rocks of the Kolyuchinskaya Bay (4); diabase and gabbro from the vicinities of Bilibino and Cape Schmidt (5). Dolerite of the New Siberian Islands (6).

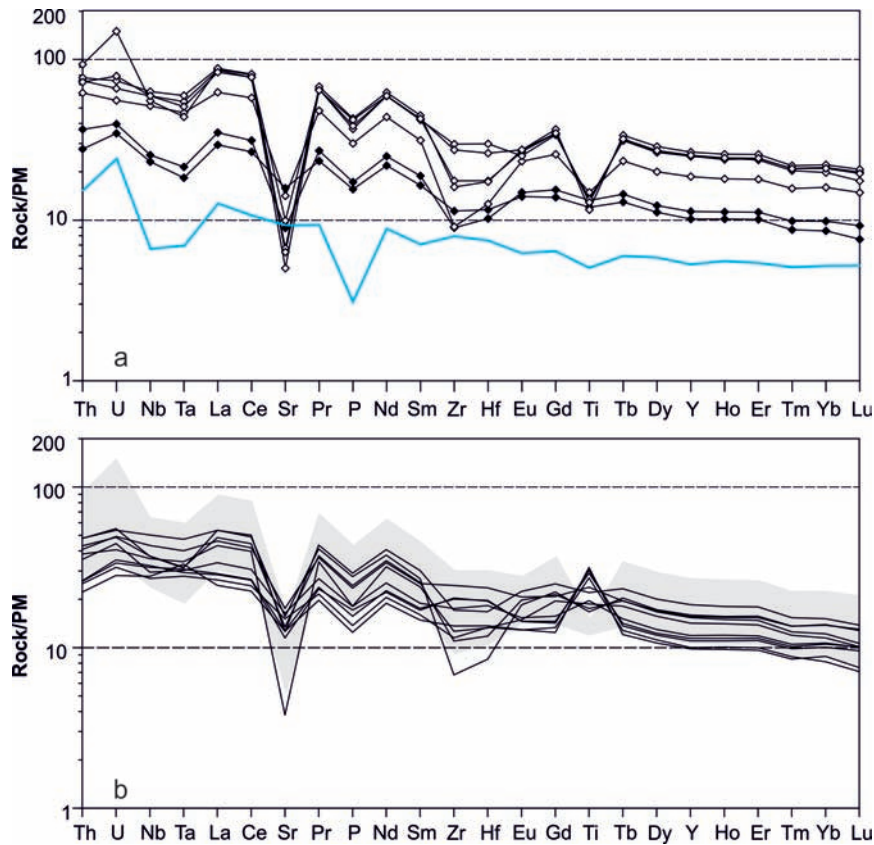


Fig. 8. Multi-element diagrams of primitive mantle (PM) normalized (Sun and McDonough, 1989) trace elements of the Anyui province gabbroic rocks. For comparison the averaged spectrum of the most basalts of the trap stage of the Siberian LIP (data from Krivolutskaya, 2013) is shown. **(a)** gabbro (filled diamonds) and gabbroic diorites (open diamonds) probably free of the admixed cumulative Fe-Ti oxides; **(b)** Fe-Ti gabbro in the comparison with gabbro and gabbroic diorite (the grey field).

ments were performed at the Geological Institute of the Kola Research Center of the Russian Academy of Sciences, Apatity, Russia with a Finnigan MAT-262 (RPQ) seven channel mass spectrometer employing the method described in detail by Bayanova (2004). During the course of measurements, the laboratory blank was lower than 0.3 ng Nd and 0.06 ng Sm. The international standard (La Jolla) gave ratios of $^{143}\text{Nd}/^{144}\text{Nd} = 0.511851 \pm 17$ (N=20). The uncertainty of the $^{147}\text{Sm}/^{144}\text{Nd}$ ratio was calculated from twenty measurements of Sm and Nd concentrations in the BCR-1 standard as 0.2% (2σ). The measured Nd isotopic ratios were normalized to $^{148}\text{Nd}/^{144}\text{Nd} = 0.241570$ and then adjusted to the value $^{143}\text{Nd}/^{144}\text{Nd} = 0.511860$ in the La Jolla standard. The decay constants were taken from Steiger and Jaeger (1977).

Results of the Sm-Nd isotope investigations

Results of Sm-Nd isotope measurements are

presented in Table 5. The gabbro, Fe-Ti gabbro and gabbroic diorite of the Anyui province of eastern Chukotka display positive $\epsilon\text{Nd}(t=252 \text{ Ma})$ ranging from +2.8 to +1.2. ϵNd values are well correlated with MgO contents for rocks from the areas of the Gytgyl'ven pass and Ploskaya River in western Chukotka and are lowered as MgO decreases (Fig. 9).

INTERPRETATION OF $^{40}\text{Ar}/^{39}\text{Ar}$ AGES

Sample GY9-87, gabbroic diorite of the Anyui dike-and-sill province, contains hornblende whose composition (Table 3, column 41) is close to a magmatic composition of this mineral. Despite this, the late Triassic $^{40}\text{Ar}/^{39}\text{Ar}$ plateau age of this hornblende can be hardly regarded as the time of rock crystallization. The gabbroic rocks of the Anyui province (including the sample studied) are not younger than the Early-Middle Triassic as they are folded and metamorphosed together with Permo-

Table 5. Sm-Nd isotopic composition of plutonic rocks of the Anyui province

Sample	Sm, ppm	Nd, ppm	$^{147}\text{Sm}/^{144}\text{Nd}$	$^{143}\text{Nd}/^{144}\text{Nd}$	Err	$\epsilon\text{Nd}(t=252 \text{ Ma})$
GY9-101	6.479	26.236	0.149257	0.512662	0.000007	2.2
GY9-74	6.179	24.204	0.154296	0.512702	0.000004	2.8
GY9-76	12.810	51.699	0.149769	0.512638	0.000012	1.7
GY9-82a	12.899	54.411	0.143289	0.512662	0.000021	2.4
GY9-87	18.685	76.994	0.146686	0.512604	0.000008	1.2
KE9-73	6.726	26.280	0.154700	0.512642	0.000016	1.6
KE9-71	7.172	28.155	0.153968	0.512621	0.000008	1.2
PS9-89	7.928	31.920	0.150115	0.512664	0.000007	2.2
PS9-90	10.998	46.800	0.142047	0.512635	0.000007	2.0
PS9-92	7.561	30.884	0.147980	0.512663	0.000005	2.3

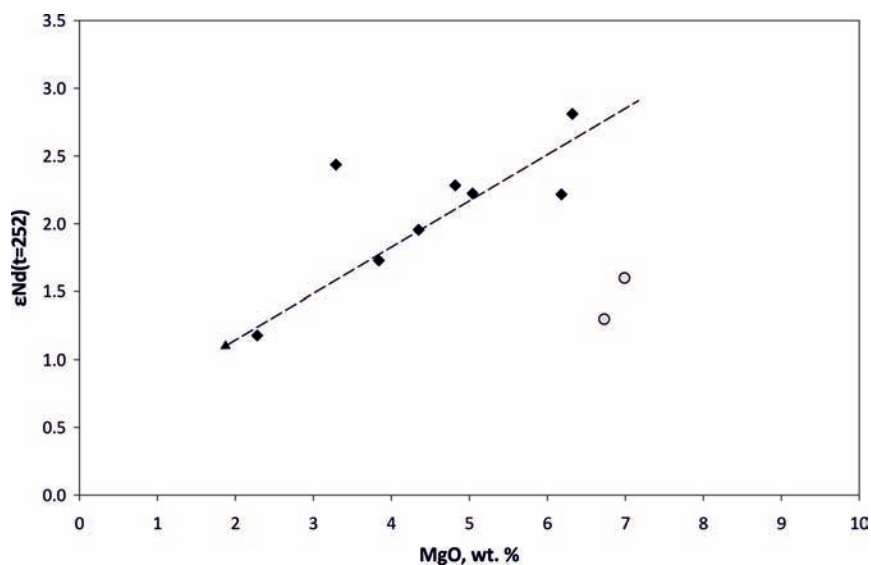


Fig. 9. MgO, wt. % vs. $\epsilon\text{Nd}(t=252 \text{ Ma})$ plot for rocks of the Anyui province of eastern Chukotka. Symbols correspond to gabbroic rocks of the Gytgyl'ven pass and Ploskaya River domains (black diamond) and the Kolyuchinskaya Bay domain (grey circle). Sm-Nd data for the Kolyuchinskaya Bay area are from Ledneva, et al. (2011).

Triassic and Early-Middle Triassic strata hosting them, and they do not intrude Late Triassic and younger deposits. In general, $^{40}\text{Ar}/^{39}\text{Ar}$ plateau age of $218.3 \pm 5.2 \text{ Ma}$ (Norian) might be considered as the cooling age of the gabbro to a temperature of $\sim 500 \pm 50^\circ\text{C}$, e.g. an argon closure temperature in hornblende (McDougall and Harrison, 1999). An alternative interpretation is the resetting of the argon isotope system in the hornblende without influencing its major-element composition.

In sample PS9-89 of gabbro, the primary

hornblende is preserved only as a relict mineral (Table 3, column 46), and it is largely replaced by actinolite. The $^{40}\text{Ar}/^{39}\text{Ar}$ plateau age of $167.8 \pm 11.2 \text{ Ma}$ (Middle Jurassic) might therefore reflect an argon system reset during a metamorphic event. Igneous zircons from this sample yielded U-Pb LA-ICPMS age corresponding to the Middle Triassic (V.L. Pease, personal comm.).

The confines of the Anyui province rocks to Permo-Triassic and lower-middle Triassic shelf sediments of Chukotka, joint deformations of

dikes and sills with hosting them strata and U-Pb TIMS age of igneous zircons from gabbro of the Kolyuchinskaya Bay indicate that gabbroic rocks of the Anyui dike-and-sill province are Permo-Triassic to Early-Middle Triassic in age. The upper Triassic $^{40}\text{Ar}/^{39}\text{Ar}$ plateau age (218.3 ± 5.2 Ma) of hornblende is correlated with Norian magmatism which is recorded in basaltic lavas and gabbroic diorite sills (Tynankergav and Bychkov, 1987; V.L. Pease, personal comm.) of the Vel'may terrane. The tabular body dated is too thin (about 30 meters thick) to cool slowly. So we suggest that the Norian age of hornblende probably reflects a thermal event that resulted in the resetting of the argon isotope system in hornblende without influencing its major-element composition. We are unable to distinguish whether rocks of the Anyui province originated in a single or several magmatic episodes, and we assume that the studied rocks of eastern Chukotka to be coeval to each other.

PETROLOGICAL AND GEOCHEMICAL INTERPRETATIONS

An interpretation of the mineralogical data

In mg# vs. major-element oxide, wt. % plots for clinopyroxene and hornblende (Fig. 4 and 5) compositions of the minerals display linear trends. This might be indicative of a cogenetic nature of gabbro, Fe-Ti gabbro and gabbroic diorite from different bodies of the Anyui province because of the following. Abundances of both clinopyroxene and hornblende in alumina are generally sensitive to a pressure of magma crystallization. In binary diagrams, the hornblende studied follows a linear trend. This suggests crystallization of gabbro, Fe-Ti gabbro and gabbroic diorite from different tabular bodies at similar pressure or depth, which is consistent with pressure estimates as discussed below. Augite is characterized by two levels of alumina abundances (1.14-2.09 and 3.02-3.63 wt. %, Al_2O_3). Low-Al augite occurs in all samples (the only exclusion is the sample PS9-92) and forms a continuous trend of Al_2O_3 decrease with mg# decrease. This suggests a primary magmatic nature of low-Al augite and its crystallization along with plagioclase at a similar pressure in different bodies. Augite showing moderate alumina contents (samples PS9-89 and PS9-92 from the same tabular body, P-11-7a) occurs

in the body whose rocks contain low-Al augite as well. Augites with higher Al_2O_3 contents probably crystallized at a deeper level while augites with lower Al_2O_3 contents probably originated in situ in tabular bodies.

Abundances of clinopyroxene in titanium and sodium and of hornblende in titanium and potassium depend on the composition of (parent magma) equilibrium melt (e.g. Zlobin and Zakariadze, 1993) and P-T parameters of crystallization. In low-Al augite, TiO_2 contents decrease as mg# decreases. In hornblende, TiO_2 and K_2O contents slightly increase as its mg# decrease. These binary diagrams show that low-Al augite of rocks from different bodies form one trend. This is also true for hornblende. Using the mg# of the minerals as a measure of a magma differentiation degree, we conclude that different bodies were probably originated from portions of variably differentiated magmas derived from some initial melts similar in titanium, sodium and potassium contents, and crystallization of these magmas in situ took place at similar pressure and temperature conditions.

Conditions of crystallization

Pressures of rock crystallization are estimated by aluminum-in-hornblende geobarometer of Schmidt (1992) and range from 1.2 to 3.4 kbar. Pressures calculated by aluminum-in-hornblende geobarometer of Ridolfi, et al. (2009) are 0.9 ± 0.2 kbar. Although the geobarometer of Schmidt is calibrated for clinopyroxene-free assemblages and the geobarometer of Ridolfi, et al. (2009) is calibrated for volcanic hornblendes, close similarity of calculated pressures suggests that the studied rocks crystallized at very low pressures.

Equilibrium temperature for augite-pigeonite pairs (in samples KE9-73 and T-05-5) was calculated using the QUILF program (Anderson, et al., 1993) and corresponds to about $900\text{-}910(\pm 20)^\circ\text{C}$ and $840\text{-}860(\pm 50)^\circ\text{C}$ for core and rim pyroxene compositions at a pressure of 2 kbar. Temperatures of primary hornblende crystallization are estimated based on the equation of Ridolfi, et al. (2009) and vary from 710 to 780°C . In one of the samples (GY9-82a) we also estimated equilibrium temperature of coexisting hornblende with mg# of 34.2 and oligoclase with $\text{xAn}_{22.6}$ composing outer rims of grains in

contact using the geothermometer of Holland and Blundy (1984). The estimated temperature is about 720°C (for 2 kbar). A large interval of equilibrium temperatures in a single sample reflects a relatively fast rock cooling and is consistent with their crystallization at the low pressure.

An oxygen fugacity estimated by the method of Ridolfi, et al. (2009) varies from -13.2 to -15.1 which correspond to $\Delta\text{NNO}+0.4$ to $\Delta\text{NNO}+1.1$. H_2O contents in melts coexisting with hornblendes are estimated at 3.3-5.7 wt. % (Ridolfi, et al., 2009). These results are not very reliable as this calibration is proposed only for hornblendes from subduction-related lavas.

All these estimations are related to the stage of in situ rock crystallization. Crystallization at a deeper level can be inferred from the fact that rocks composing different bodies are variably differentiated and there are no signs of in situ fractionation. A pressure for the previous crystallization stage can be roughly evaluated from composition of clinopyroxenes with elevated Al_2O_3 contents (Fig. 4); estimations by the method of (Putirka, 2008) give a pressure of 4 ± 2 kbar.

Imprints of admixed cumulative minerals

The rocks studied show a strong correlation of immobile incompatible trace elements (REE, P, Nb) both with each other and with some major elements (Si, Al, Mg) as well. This suggests that rock compositions are generally similar to the compositions of the melts, and an admixture of cumulate minerals is moderate. However, it was not negligible for most of rocks. This is demonstrated by evidently elevated contents of Ti, Fe, V, which are correlated with each other but are not correlated with contents of other elements. These covariations suggest a variable amount of cumulate Fe-Ti oxide grains suspended in the melts.

Admixed cumulate Fe-Ti oxides in bulk rocks can be predicted based on comparison of titanium and REE contents. Among REE titanium has bulk distribution coefficient (a restite or cumulate to a melt) similar to Dy and Gd which is obvious from Ti/Gd and Ti/Dy ratios. These ratios are similar in different primitive mantle-derived melts (N-MORB, E-MORB and subduction melts), primitive ultramafic and mafic cumulates and in mantle sources (Sun and

McDonough, 1989; Hofmann, 1988; Kelemen, et al., 2003). These elements behave similarly during both mantle melting and melt fractionation (in the absence of Fe-Ti oxides) and normalized to primitive mantle ratio of $(\text{Ti}/\text{Gd})_N$ and $(\text{Ti}/\text{Dy})_N$ is ~ 1 in both melts and cumulates. Fe-Ti oxides will fractionate this ratio and an addition of cumulate Fe-Ti oxides will raise this ratio ($(\text{Ti}/\text{Gd})_N > 1$, $(\text{Ti}/\text{Dy})_N > 1$), while an extraction of Fe-Ti oxides will lower the ratio ($(\text{Ti}/\text{Gd})_N < 1$, $(\text{Ti}/\text{Dy})_N < 1$) (Kelemen, et al., 2003). Thus, Gd vs. TiO_2 plot can be useful to separate effects of Fe-Ti oxides addition and extraction to melts. However, Gd contents in rocks are affected with an addition of Fe-Ti oxides while the Gd/SiO_2 ratio remains constant. In Gd/SiO_2 vs. $\text{TiO}_2/\text{SiO}_2$ diagram (Fig. 10) bulk compositions of rocks with the lowest TiO_2 concentrations form trend that probably reflects evolution of melt saturated in Fe-Ti oxides. At initial stages of crystallization (before melt saturation in Fe-Ti oxides) melt compositions probably evolve along the line corresponding to $(\text{Ti}/\text{Gd})_N = 1$. Rock samples plotting above these trends are interpreted to be a mixture of melt and cumulative Fe-Ti oxides.

The amount of these phases can be evaluated from the quantity of excess Ti and Fe over the level

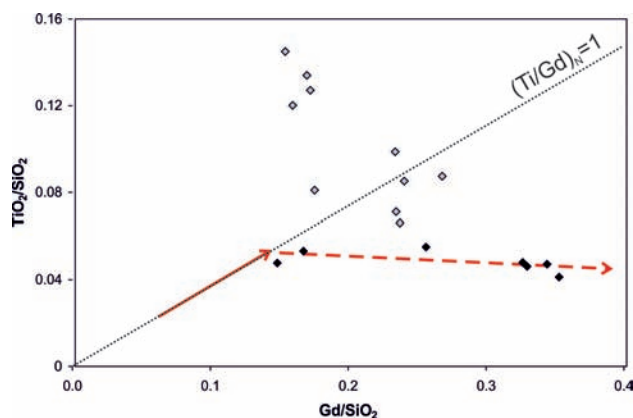


Fig. 10. Covariations of Gd and TiO_2 in bulk rocks. Contents of Gd (ppm) and TiO_2 (wt. %) are normalized to SiO_2 (wt. %). Black diamond is the symbol for the gabbro and gabbroic diorite with the lowest TiO_2 contents; grey diamond is the symbol the Fe-Ti gabbro. The solid arrow corresponds to a probable melt evolution before melt saturation in Fe-Ti oxides; the dashed arrow shows probable melt evolution after melt saturation in Fe-Ti oxides. The excess of titanium in the Fe-Ti gabbro relative to the level of melt saturation in Fe-Ti oxides is attributed to various amounts of admixed cumulative Fe-Ti oxides in the rocks.

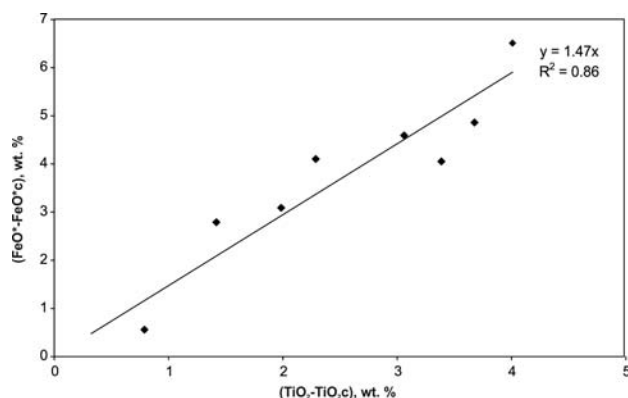


Fig. 11. Correlation of excess amounts of TiO_2 and FeO^* in the Fe-Ti gabbro demonstrating nearly constant ratio of Ti-magnetite/ilmenite in cumulate Fe-Ti oxides.

of melt saturation in respect to these elements (see Appendix for details of calculations). In the Fe-Ti gabbros studied, the excess quantities of Ti and Fe display a good correlation (Fig. 11), which indicates FeO/TiO_2 value of 1.47. This value corresponds to Ti-magnetite/ilmenite ratio of 0.3/0.7 in the rocks (if the average compositions of these minerals are used), which is supported by petrographic observations.

Some rocks studied show chemical imprints of a possible addition not only of Fe-Ti oxides but also of cumulative silicate phases. Samples GY9-99 and GY9-102 display anomalously high MgO contents that can be attributed to significant amounts of cumulative magnesium clinopyroxenes or orthopyroxenes. Samples GY9-99, PS9-92 and GY9-101 have slightly elevated bulk-rock Cr contents, which can be indicative of admixture of pyroxenes with detectable Cr contents (Table 3). However, we cannot numerically estimate the quantity of cumulative silicates in these rocks as we don't know the composition of admixed cumulative minerals.

Mobility of elements due to metamorphism

Bulk rock compositions were modified due to metamorphism. This is evident from comparison of contents of alkali elements, Ba and Ca with both contents of immobile incompatible elements and contents of major elements (Si, Al, P) (Fig. 12). Metamorphic replacements of biotite suggest the potassium loss. Relicts of primary biotite are preserved only in the freshest samples and its metamorphism does not usually result in potassium-

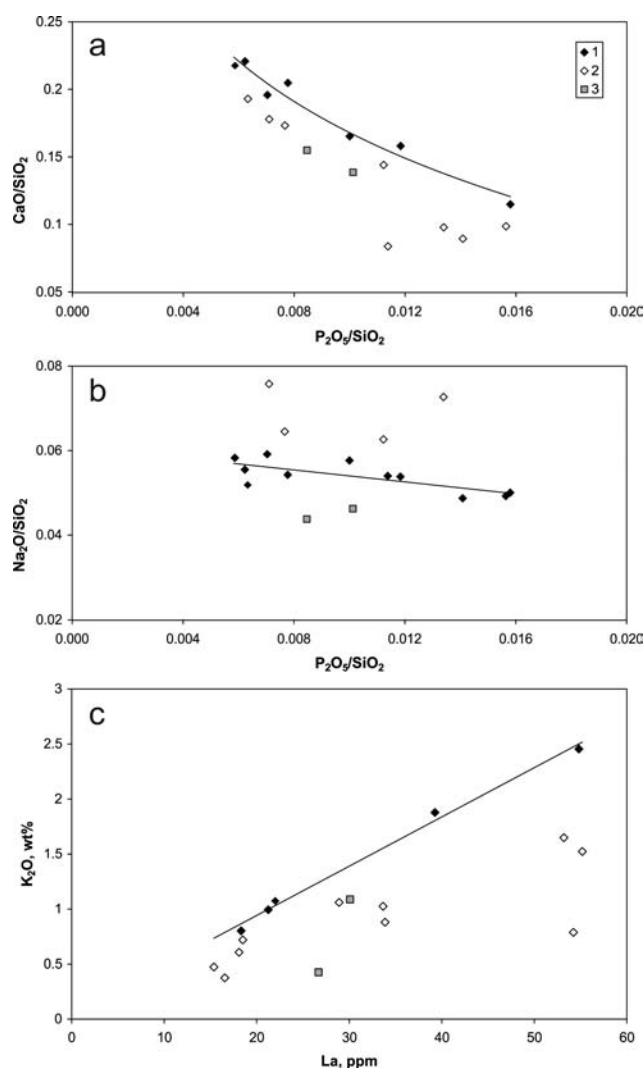


Fig. 12. The diagrams demonstrating the loss of calcium (a), gain of sodium (b) and loss of potassium (c) during metamorphic alteration of rocks. Black diamond (1) corresponds to the rocks probably characterized by primary element abundances; open diamonds (2) are allochemically (in respect to a considered element) metamorphosed rocks; grey squares (3) are rocks with significant admixture of silicate phases or strongly allochemically metamorphosed.

rich minerals. Stilpnomelane after biotite, which contains a much lower potassium contents, is rather rare and was found only in a few samples. Clinopyroxene replacement by secondary amphibole and plagioclase replacement by albite, which are common in the rocks studied, suggest the likelihood of calcium loss. Thus, potassium contents close to original (e.g. existed prior to metamorphism) concentrations of this element in rocks are expected to remain only in samples with the highest ratios of potassium to high incompatible elements such

as K/La. Calcium contents close to its original concentrations in rocks are expected in samples with the highest ratios of calcium to moderate incompatible or moderate compatible immobile elements such as CaO/SiO_2 and $\text{CaO}/\text{Al}_2\text{O}_3$. Sodium behavior is not clear from petrography. As various binary correlations indicate, sodium contents in most of the rocks are close to its original concentrations. Only a few samples have elevated sodium concentrations; which can be attributed to plagioclase albitization. In several rocks studied, Ca, K, Rb, Ba (and probably Sr) were removed and Na was added during metamorphism. In general, this tendency is typical for sea-floor spilitization. Hence, the contents of alkali elements and Ca in the rocks should be corrected to reconstruct original rock compositions prior to metamorphism that should be used for evaluation of the modal mineral modes of the rocks and a correct rock chemical and mineralogical classification.

Primary bulk rock chemical and modal mineral compositions

The original contents of calcium, sodium and potassium in the rocks were evaluated using a set of binary element correlations of the same type as demonstrated in the Appendix. For mineral mode calculations, the real mineral compositions (averaged or generalized) (Table 3) were used. The calculations were performed by the least square sum minimization procedure for optimization using a difference between real and calculated oxide contents normalized to the probable value of the integrated analytical uncertainty (both XRF for bulk rock and electron microprobe for minerals). In the calculations, wt. % contents of SiO_2 , TiO_2 , Al_2O_3 , $\text{FeO}_{\text{total}}$, MgO , CaO , Na_2O , K_2O and P_2O_5 were used. In order to make the calculations some assumptions were required. Fe-Ti oxides were treated as a single phase with a composition reflecting the Ti-magnetite/ilmenite ratio of 0.3/0.7. Pigeonite and orthopyroxene were excluded from the calculations (based on their scarcity in the rocks studied). Instead of using both the compositions of anorthoclase and probable igneous orthoclase, an average composition of pure orthoclase was used. To choose compositions of clinopyroxene and biotite for each sample, we used correlations between measured compositions

of these minerals and wt. % MgO in the bulk rock. Integral composition of plagioclase in the rocks was estimated from relative quantities of xAn-rich and xAn-poor plagioclase that were used in calculations as distinct phases. Optimization was reached by varying the integral hornblende composition (along the trend demonstrated by real compositions). The results of calculations are presented in Table 6.

These data are consistent both with real assemblages of primary minerals in the rocks and with measured compositions of hornblende and plagioclase (where they were analyzed). As demonstrated in Table 6, the content of clinopyroxene is below 10% in gabbro and mainly below 5% in gabbroic diorites. The amount of Fe-Ti oxides is 3.5-5.2 % in gabbro and gabbroic diorite, and 6.0-14.2 % in Fe-Ti gabbro. Contents of orthoclase are below 4 % in gabbro and 5-9 % in gabbroic diorite. Contents of biotite are below 10 % in gabbro and 5-13% in gabbroic diorites.

Calculation of melt compositions

The procedure of reconstruction of original calcium, sodium and potassium contents in the rocks prior to metamorphism is a first step to approach probable melt composition for the rocks studied. The second step is eliminating the influence of cumulative Fe-Ti oxides on the bulk composition of Fe-Ti gabbro. To do this, we used a set of binary correlations of iron, titanium, manganese, vanadium and niobium (i.e. components showing elevated contents in the Fe-Ti gabbro relative to the gabbro and gabbroic diorite low in titanium) with both major oxides (SiO_2 , Al_2O_3 , MgO) and immobile trace elements in rocks which were probably free of cumulative Fe-Ti oxides (i.e. gabbro and gabbroic diorite). The results of these calculations are shown in Table 7 (see Appendix for details of the calculations) demonstrate a similarity of probable melt compositions calculated for gabbro, gabbroic diorite and Fe-Ti gabbro (Fig. 6 and 13). The resulting calculations for samples GY9-99 and GY9-102 do not correspond to melt compositions, probably because these rocks contain abundant cumulative silicate minerals or underwent loss/gain not only CaO , Na_2O and K_2O but other major elements as well.

Despite this, the calculations for the Fe-Ti

Table 6. Calculated modal mineral composition of the rocks (wt. %) and integral average compositions of hornblende and plagioclase

#	Sample	Rock group	Rock (QAPF)	Cpx	Hbl	Bi	Pl	Ksp	FTO	Qtz	Ap	Mg# Hbl	xAn Pl
1	GY9-74	FTG	D	5.6	47.7	1.8	29.7	0.4	14.2	0.0	0.6	50	48
2	GY9-79	FTG	D	9.5	43.8	1.8	30.6	1.0	12.0	0.7	0.7	49	49
3	GY9-101	G	Qtz G	6.1	45.7	2.6	35.6	1.1	4.2	4.0	0.8	50	54
4	KE9-71	FTG	Qtz D	2.5	41.5	2.1	35.8	1.0	13.2	3.0	0.8	51	49
5	PS9-92	G	Qtz D	4.3	42.0	3.5	38.4	1.8	4.9	4.2	0.9	44	48
6	PS9-89	FTG	Qtz D	2.2	47.5	2.4	33.3	1.6	8.0	4.0	0.9	44	48
7	KE9-73	FTG	Qtz G	5.2	39.4	2.7	33.4	1.4	13.7	3.3	0.9	49	52
8	GY9-102*	FTG	Qtz G	2.0	48.6	8.3	27.6	1.2	6.1	4.8	1.2	47	55
9	GY9-81	FTG	Qtz D	2.0	41.9	5.7	31.1	2.0	9.9	6.2	1.3	37	39
10	PS9-90	FTG	Qtz D	4.8	37.7	9.5	32.2	1.6	6.0	6.8	1.5	38	40
11	GY9-82a	D	Qtz MD	1.7	39.0	6.4	31.5	4.7	5.2	9.9	1.6	32	36
12	GY9-76	FTG	Qtz MD	8.4	36.4	5.7	26.8	4.0	9.0	8.1	1.6	33	29
13	GY9-78	D	Qtz MD	3.7	31.1	5.5	30.4	9.3	4.7	13.2	2.1	30	28
14	GY9-82b	D	Qtz MD	1.8	32.3	8.0	27.7	7.9	4.7	15.2	2.2	26	28
15	GY9-84	D	GD	1.5	32.4	13.5	26.6	5.2	4.0	14.3	2.4	26	24
16	GY9-87	D	GD	3.5	31.7	12.0	25.2	6.6	3.4	15.1	2.5	23	19

Notes: FTG – Fe-Ti gabbro, G – gabbro, D – diorite, B – basalt, Rock (QAPF) corresponds to the rock named in accordance with the QAPF nomenclature of plutonic rocks (Streckeisen, 1974, 1976). Qtz G – quartz gabbro, Qtz D – quartz diorite, Qtz MD – quartz monzodiorite, GD – granodiorite. For mineral abbreviations see the caption to Figure 3. * is rocks containing cumulative silicate minerals.

Table 7. Calculated melt compositions

#	1	2	3	4	5	6	7
Sample	GY9-101	PS9-92	GY9-74	GY9-79	KE9-71	PS9-89	KE9-73
Rock	G	G	FTG	FTG	FTG	FTG	FTG
Melt	Bas	Bas	Bas	Bas	Bas	Bas	Bas
SiO ₂	50.37	50.30	48.99	49.16	49.75	50.54	49.72
TiO ₂	2.40	2.67	2.49	2.48	2.58	2.58	2.56
Al ₂ O ₃	13.68	14.25	13.06	12.89	14.22	13.59	13.92
FeO	13.08	13.78	13.61	13.68	13.68	13.89	13.65
MnO	0.175	0.174	0.166	0.178	0.178	0.176	0.182
MgO	6.13	4.83	7.07	6.86	5.66	5.25	5.71
CaO	10.47	9.61	10.66	10.85	9.74	9.69	10.18
Na ₂ O	2.61	2.90	2.86	2.73	2.94	2.84	2.70
K ₂ O	0.74	1.11	0.82	0.86	0.89	1.06	0.99
Cr ₂ O ₃	0.019	0.012	0.000	0.000	0.000	0.002	0.000
P ₂ O ₅	0.319	0.357	0.287	0.306	0.350	0.387	0.387
Sum	100.00	100.00	100.00	100.00	100.00	100.00	100.00
Mg#	45.5	38.4	48.1	47.2	42.5	40.2	42.7

Table 7. (continued).

#	8	9	10	11	12	13	14
Sample	GY9-99*	GY9-81	GY9-102*	PS9-90	GY9-76	GY9-82a	GY9-78
Rock	FTG	FTG	FTG	FTG	FTG	D	D
Melt		Bas		Bas	AB	AB	AB
SiO ₂	44.21	51.66	48.31	50.85	53.00	52.75	55.96
TiO ₂	<u>2.18</u>	<u>2.58</u>	<u>2.42</u>	<u>2.54</u>	<u>2.50</u>	2.90	2.58
Al ₂ O ₃	10.96	13.10	12.48	12.88	11.44	12.62	12.29
FeO	<u>18.91</u>	<u>14.84</u>	<u>16.61</u>	<u>15.70</u>	<u>15.25</u>	15.47	13.57
MnO	<u>0.141</u>	<u>0.174</u>	<u>0.164</u>	<u>0.173</u>	<u>0.171</u>	0.171	0.138
MgO	8.78	4.13	5.97	4.35	4.02	3.18	2.53
CaO	<u>10.78</u>	8.53	<u>9.45</u>	<u>8.49</u>	8.38	<u>7.58</u>	<u>6.82</u>
Na ₂ O	2.40	2.98	2.68	<u>2.80</u>	2.85	2.85	<u>2.90</u>
K ₂ O	<u>1.24</u>	<u>1.49</u>	<u>1.43</u>	<u>1.65</u>	<u>1.77</u>	1.88	<u>2.46</u>
Cr ₂ O ₃	0.015	0.000	0.006	0.005	0.000	0.002	0.000
P ₂ O ₅	0.374	0.517	0.489	0.571	0.628	0.600	0.749
Sum	100.00	100.00	100.00	100.00	100.00	100.00	100.00
Mg#	45.3	33.2	39.0	33.1	32.0	26.8	25.0

Table 7. (continued).

#	15	16	17
Sample	GY9-82b	GY9-87	GY9-84
Rock	D	D	D
Melt	AB	AB	AB
SiO ₂	55.76	55.58	54.50
TiO ₂	2.67	2.29	2.57
Al ₂ O ₃	11.83	11.13	11.58
FeO	14.85	16.00	16.29
MnO	0.144	0.205	0.192
MgO	2.27	2.23	2.44
CaO	<u>6.47</u>	<u>6.29</u>	6.26
Na ₂ O	2.72	2.74	2.73
K ₂ O	2.49	<u>2.66</u>	<u>2.58</u>
Cr ₂ O ₃	0.000	0.000	0.001
P ₂ O ₅	0.785	0.870	0.861
Sum	100.00	100.00	100.00
Mg#	21.4	19.9	21.0

Notes: Corrected values are underlined. * is samples probably containing cumulative silicates along with Fe-Ti oxides, contents of FeO* and CaO in melts are poorly constrained. Bas – melts of the basaltic composition, AB – melts of basaltic andesitic composition. See Appendix for the details of calculations.

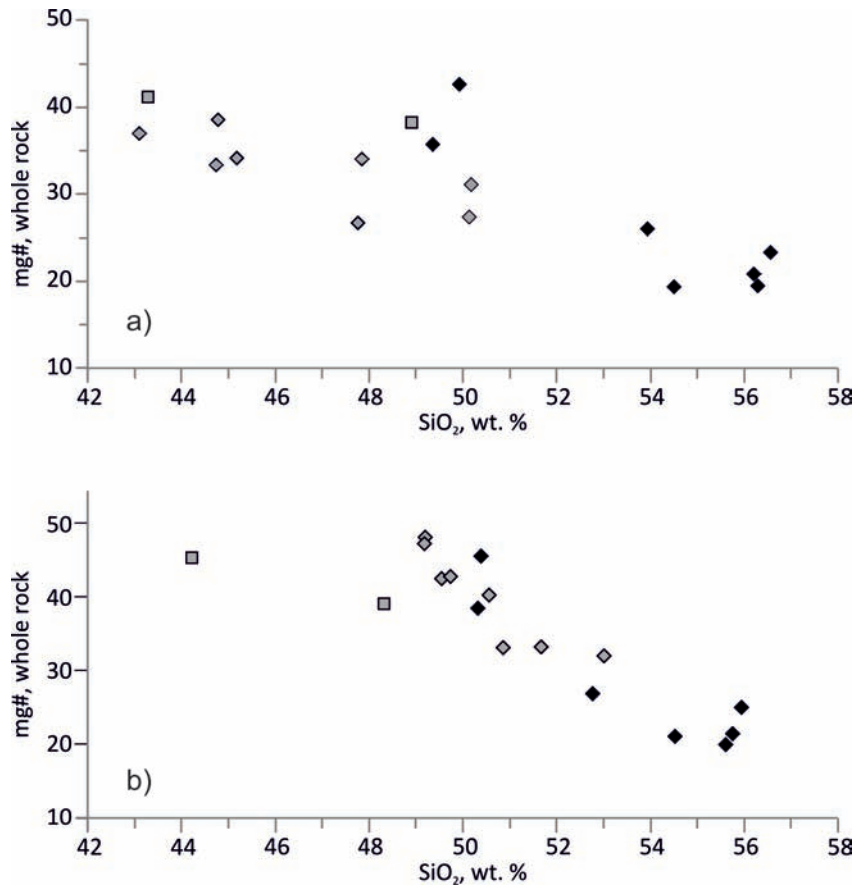


Fig. 13. SiO₂ vs. mg# of whole rocks (a) and SiO₂ vs. mg# of calculated melts (b) for rocks of the Anyui province of eastern Chukotka. Black diamond (1) corresponds to the gabbro and gabbroic diorite; grey diamond (2) is the Fe-Ti gabbro; grey square (3) is rocks with significant admixture of silicate phases or strongly allochemically metamorphosed.

gabbro excess contents of manganese, vanadium and niobium demonstrate good correlation with excess content of titanium. This is in accordance with assumption that contents of these elements in bulk rocks are influenced by admixed cumulative Fe-Ti oxides. It can be inferred from these correlations that the content of MnO in the bulk Fe-Ti oxide consists of 0.85 wt. %, that of V₂O₃ is 0.65% and that of Nb is about 60 ppm.

Figure 13 demonstrates covariations of SiO₂ and mg# of measured whole rock compositions and calculated melts. In comparison with calculated melts, actual rocks show a wider range of SiO₂ and Fe-Ti gabbros are generally lower in SiO₂ contents. This reflects their abundances in Fe-Ti oxides as discussed above. Parent melts for gabbro, Fe-Ti gabbro and gabbroic diorites form trend

of increasing SiO₂ with decreasing mg# which suggests that all rocks investigated originated from melt portions via crystal fractionation of magmas of similar compositions. Compositions of parent melts for gabbros fall into the range of parent melts for Fe-Ti gabbros. The least differentiated melts formed the Fe-Ti gabbro (samples GY9-74 and GY9-79) of the Anyui province in eastern Chukotka which were basaltic with SiO₂ ~49 wt. % and mg# ~47-48. These basaltic compositions are far from primitive (i.e. equilibrated with residual mantle peridotites) and suggests primary melt differentiation in a deeper magma-chamber. The degree of crystal fractionation of the most differentiated gabbroic diorites was probably up to 60-65%, inferred from enrichment in highly incompatible elements (La, Ce) relative to parental melt (sample GY9-74) (see the Appendix).

In the TAS diagram (Fig. 6a) for plutonic rocks and SiO_2 vs. K_2O plot for volcanic rocks (Fig. 6b) alkali elements exhibit irregular variations in measured rock samples because of mobility of sodium and potassium in the metamorphic process as discussed above. This prevents the correct definition of rock series affinity from bulk rock compositions. In contrast, calculated melts form systematic trends showing the affinity of calculated melts to moderately alkaline series. Basaltic compositions (calculated from most of the gabbro and Fe-Ti gabbro) belong to medium-potassium (calc-alkaline) series and basaltic andesite compositions (calculated from gabbroic diorites) belong to high-potassium (shoshonitic) series.

Interpretation of Sm-Nd isotope

Sm-Nd isotopes indicate that the gabbro, Fe-Ti gabbro and gabbroic diorite studied are crustally contaminated rocks. The most evolved samples show the lowest ϵNd value, which could be interpreted to reflect a greater crustal input. It is hard to distinguish whether a source or a melt at some stage of its evolution was contaminated. However assuming the rocks from the Gytgyl'ven pass and Ploskaya River domains (for which Sm-Nd data are presented here) to be coeval and cogenetic we argue that contamination of melts by crustal material could be important for these rocks. Nonetheless, it does not exclude a source contamination by a crustal material. The gabbro from the Kolyuchinskaya Bay area lies out of the trend formed by the rocks investigated, and this suggests either source heterogeneity beneath the eastern Chukotka area and/or different compositions of the source of contamination. In the Nb/Yb vs. Th/Yb and $(\text{La}/\text{Nb})_{\text{PM}}$ vs. $(\text{Th}/\text{Ta})_{\text{PM}}$ plots (Fig. 14) the gabbro, Fe-Ti gabbro and gabbroic diorite exhibit variations that are consistent with contamination of mantle-derived enriched melts either by upper crustal material or by sediments.

GEODYNAMIC INTERPRETATIONS

Geodynamic setting of the Anyui province rocks

The data on mineral and whole rock compositions presented above suggest that the investigated gabbro, Fe-Ti gabbro and gabbroic diorite from eastern Chukotka can probably be treated as cogenetic rocks derived from several portions of variably

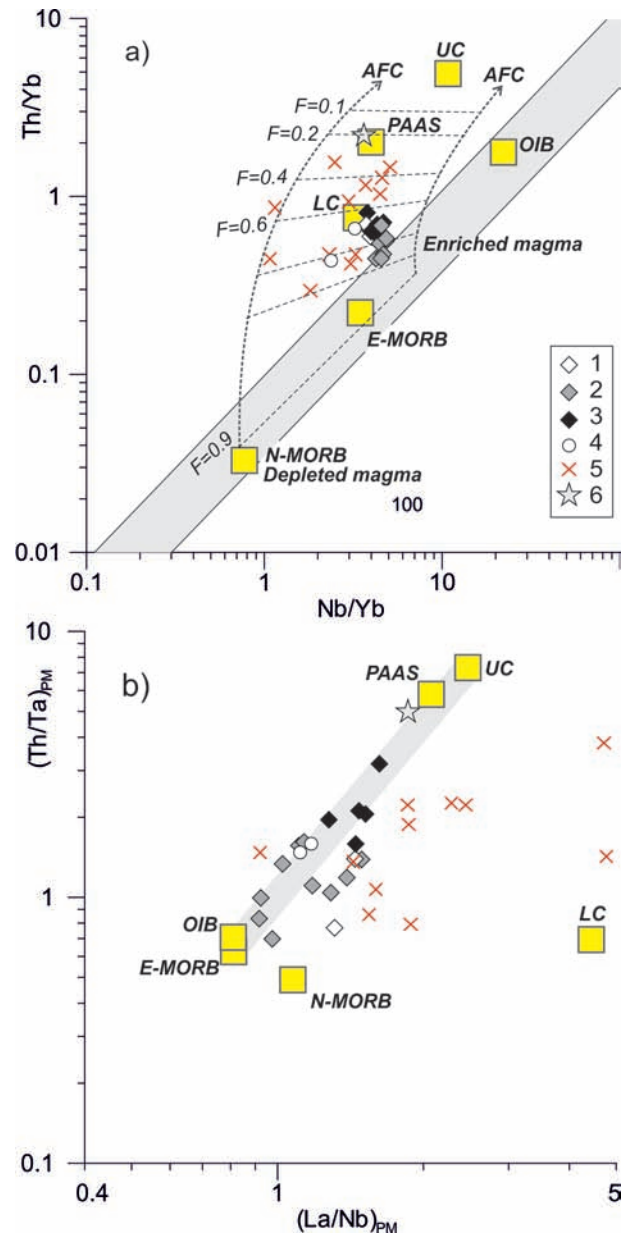


Fig. 14. Nb/Yb vs. Th/Yb (a) (Pearce, 2008) and $(\text{La}/\text{Nb})_{\text{PM}}$ versus $(\text{Th}/\text{Ta})_{\text{PM}}$ (b) (Neal, et al., 2002) diagrams, showing probable contamination of rocks of the Anyui province of eastern Chukotka by crustal material. N-MORB, E-MORB and OIB are from (Sun and McDonough, 1989); average lower crust (LC) and upper crust (UC) are from (Rudnick and Fountain, 1995); the post-Archean Australian shale (PAAS) is from (Taylor and McLennan, 1985). In plot (a), modeling curves of combined fractional crystallization and contamination (AFC) are from (Pearce, 2008). Wide grey line in plot (b) indicates probable contamination of mantle-derived enriched melts by crustal material.

Symbols 1 to 3 correspond to gabbro (1), Fe-Ti gabbro (2), gabbroic diorite (3). Other symbols are for gabbroic rocks of the Kolyuchinskaya Bay (4) and the New Siberian Islands (5), and terrigenous sediments (unpublished authors' data) hosting the investigated sills in eastern Chukotka (6).

differentiated melts of a similar initial composition. The studied rocks have compositions similar to that of the calculated melts with little or no admixture of cumulate Fe-Ti oxides (and silicates). Thus, discrimination diagrams proposed for the volcanic rocks can be generally applied for geodynamic interpretation of geochemical data. Samples GY9-99 and GY9-102 probably contain a significant amount of cumulative silicate minerals and are ignored in this summary.

The multi-element spectra (Fig. 8) and some ratios of incompatible elements (Fig. 14) are characteristic of rocks produced from enriched mantle-derived basic melts. The negative anomalies of Nb-Ta and Zr-Hf observed in the rocks can be attributed to crustal contamination, as discussed. The spectra of the rocks studied are similar in shape to that of trap basalts of the Siberian LIP (Fig. 16a) which also exhibit negative anomalies of Nb-Ta attributed to a crustal input (Lightfoot, et al., 1993; Wooden, et al., 1993; Al'Mukhamedov, et al., 1999; Medvedev, 2004; Krivolutskaya, 2013). The difference in trace-element abundance between the rocks investigated and the Siberian traps is probably due to a different degree of magma crystallization (Siberian basalts have higher mg# than the rocks investigated). In the La-Y-Nb plot (Fig. 15a) the gabbro and Fe-Ti gabbro compactly fall in the field of continental basalts; the Fe-Ti gabbro (despite admixed cumulative Fe-Ti oxides concentrating Nb) are only slightly displaced relative to the gabbro toward a more Nb-rich compositions. In the Th-Hf-Ta plot (Fig. 15b) the Fe-Ti gabbro partially lies in the field of intraplate basalts (which is indistinguishable from the field of E-MORB). Data points of the gabbro and some gabbroic diorites are displaced toward the field of subduction-related calc-alkaline lavas. This can be attributed to crustal contamination, as discussed above. Siberian trap basalts also lie in the field of arc lavas. We conclude that the gabbro, Fe-Ti gabbro and gabbroic diorite show geochemical features of continental intra-plate crustally contaminated lavas. A non-subduction origin of the Anuyi province rocks is also consistent with compositional variations of biotites that are typical of anorogenic granites but not of subduction-derived felsic rocks (Abdel-Rahman, 1994).

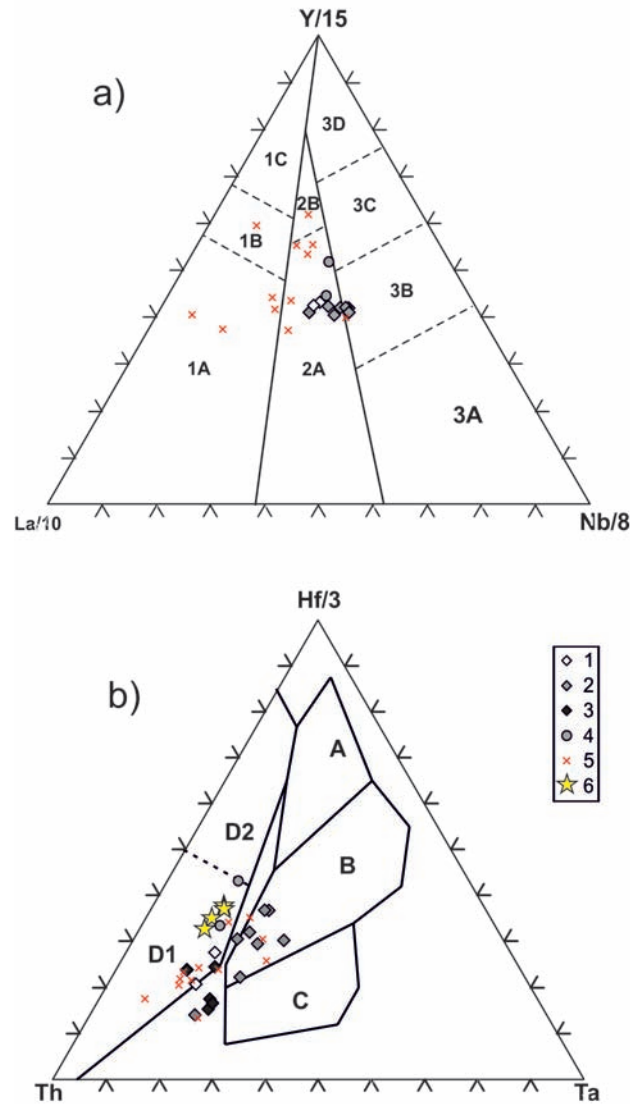


Fig. 15. Tectonomagmatic diagrams (a) La-Y-Nb (Cabanis and Lecolle, 1989) and (b) Th-Hf-Ta (Wood, 1980) for the studied rocks of eastern Chukotka.

Symbols are as follows: studied gabbro (open diamond, 1) Fe-Ti gabbro (grey diamond, 2), gabbroic diorite (black diamond, 3), gabbro of the Kolyuchinskaya Bay (grey circle, 4), rocks of the New Siberian Islands (crosses, 5) (Kuz'michov and Pease, 2007), basalts of the platformal or trap stage of the Siberian LIP (star, 6) (Al'Mukhamedov, et al., 2004; Krivolutskaya, 2013).

In plot (a) fields are as follows: 1 – basalts of the volcanic arcs (1a – calc-alkaline basalts, 1C arc tholeiites, 1B – both calc-alkaline basalts and arc tholeiites), 2 – continental basalts (2a – continental basalts, 2b – back-arc basalts), 3 – oceanic basalts (3A – alkaline basalts of continental rifts, 2b – enriched E-MORB, 3C – slightly enriched E-MORB, 3D – N-MORB).

In plot (b) fields in Fig. 14b are as follows: A – N-MORB, B – E-MORB and intraplate tholeiites, C – intraplate alkaline basalts, D1 – calc-alkaline lavas, (D2) – arc tholeiites.

REGIONAL CORRELATIONS

The material presented suggests that the shelf of the Chukotka microcontinent was an arena of intra-plate basic magmatism in the Permo-Triassic to Early-Middle Triassic time. This epoch is known for a global plate-tectonic reorganization and superplume impingements. In particular, one of such superplumes resulted in voluminous eruptions of basaltic lavas and formation of numerous mafic intrusions in the Siberian platform and West Siberian Basin referred to as the Siberian large igneous province (LIP) (e.g. Reichow, et al., 2009). In the Arctic region, manifestations of the Siberian LIP were reported in the Taimyr Peninsula, in the

islands of the Kara Sea (Vernikovskiy, et al., 2003; Dobretsov, et al., 2008) and in the New Siberian Islands (Kuz'michov and Pease, 2007).

The Anyui province rocks of eastern Chukotka are coeval to the Siberian traps in general and to the dolerite and gabbro-dolerite of the New Siberian Islands. However, rocks of eastern Chukotka and the New Siberian Islands differ in major- and trace-element chemistry (Fig. 16b). The gabbro, Fe-Ti gabbro and gabbroic diorite of eastern Chukotka from the regions investigated and from the Kolyuchinskaya Bay are much more evolved. Nonetheless the difference in geochemistry between the rocks of these two regions hardly can be

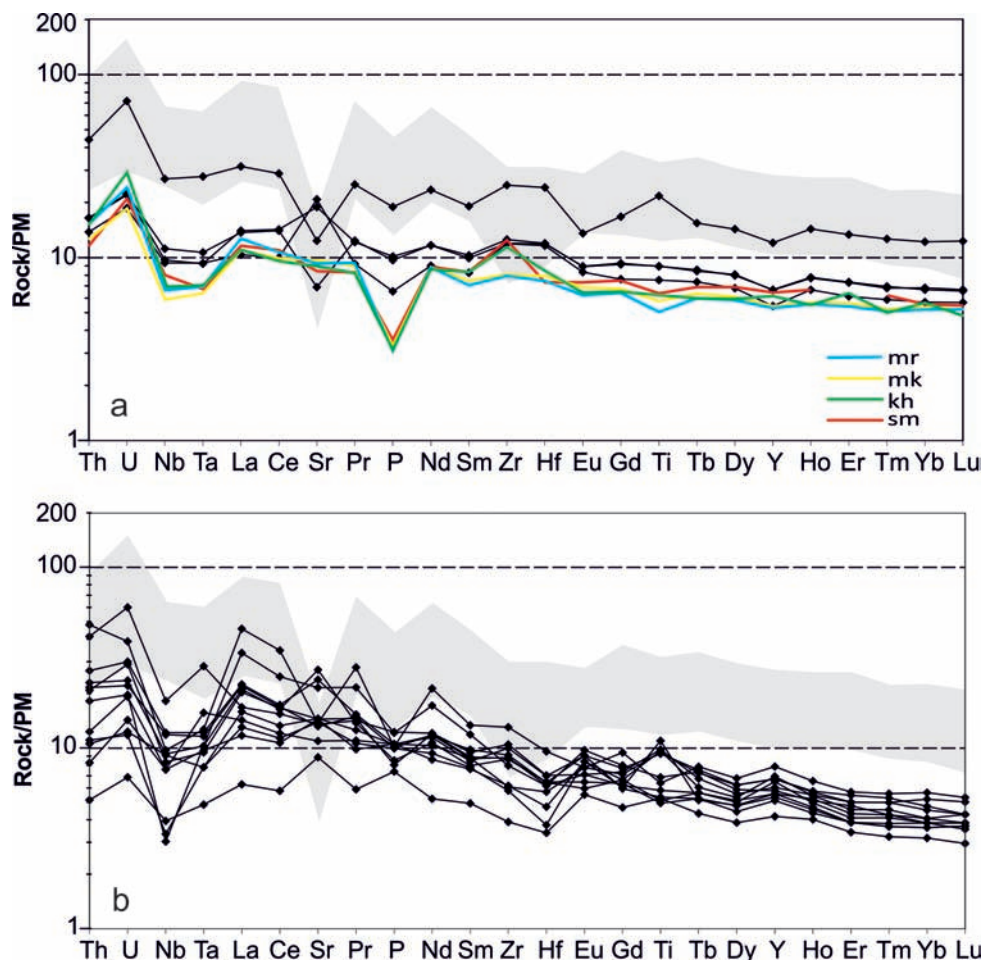


Fig. 16. Multi-element spectra shown in plot (a) demonstrate the geochemical similarity between gabbroic rocks of eastern Chukotka from the study areas and the Kolyuchinskaya Bay region (Ledneva, et al., 2011). The latter closely resembles Siberian LIP basalts of the platform or trap stage (Al'Mukhamedov, et al., 2004; Krivolutsкая, 2013), which are the most typical and widespread in the Noril'sk region (the Formations are as follows: Morongo, mr; Mokulaev, mk; Kharaelakh, kh; Samoed, sm). Plot (b) shows the difference between gabbroic rocks of eastern Chukotka and the New Siberian Islands (Kuz'michov and Pease, 2007). Normalizing values for primitive mantle (PM) are from Sun and McDonough (1989).

attributed to melt differentiation and contamination and it rather reflects a difference in sources, conditions of melting or both. To date, there are not enough data to compare rock compositions of the Anyui province from the eastern, central and western regions of Chukotka. The data on mineral composition suggest that gabbro from the vicinity of Bilibino (western Chukotka) originated from a basic melts under conditions similar to that of rocks from eastern Chukotka. As to the major elements (Fig. 7), sills and dikes from the Bilibino and Cape Schmidt areas are more similar to subvolcanic bodies of the New Siberian Islands.

In the Taimyr Peninsula and in Kara Sea, magmatism attributed to the Siberian LIP is expressed as A-type granites (Vernikovskiy, et al., 2003; Dobretsov, et al., 2008), gabbroic rocks have not been describe so far and we are unable to make comparisons.

In eastern Chukotka, the Anyui province rocks are very uniform in bulk rock geochemistry. Variations of the gabbro, Fe-Ti gabbro and gabbroic diorite studied and those from the Kolyuchinskaya Bay lie in the range of geochemical variations typical of intra-plate basalts of the platformal (Al'Mukhamedov, et al., 1999) or trap (Krivolutskaya, 2013) stage of the Siberian LIP magmatism (Fig. 16a). Analogues of the early rift picritic and basaltic lavas and the latest alkaline intrusions of the Siberian LIP are not known in Chukotka up to date. The data presented in this paper on the Anyui province rocks cannot be considered as direct evidence that the Permo-Triassic to Early-Middle Triassic intra-plate magmatism of the Chukotka microcontinent was caused by the Siberian superplume. With the same probability, the Triassic intra-plate magmatism in Chukotka could reflect an extension, which may have resulted from regional transform displacements.

ACKNOWLEDGEMENTS

This study was supported by the Russian Foundation of Basic Research (project no. 09-05-00529, 14-05-00413 and 11-05-00074), projects of FCNTP (NSH-5177.2012.5 and №14.740.11.0190), Department of Earth Sciences of RAS (program no. 10), and State contract № 01/14/20/11. We use the opportunity to thank V.V. Lebedev and A.D. Kievskiy (Georegion, Anadyr, Russia) for their help in the organization

of 2009 field studies in Chukotka. We also express our gratitude to professor Y. Hayasaka (Hiroshima University, Japan), S. Machi (Kanazawa University, Japan) and A.V. Moiseev (GIN RAS, Moscow) participated in the 2009 field studies. We cordially thank I.A. Roshchina and T.V. Romashova (GEOKHI RAS, Moscow) for analyzing whole rocks by XRF, Dr. Ya.V. Bychkova (GEOKHI RAS, Moscow) for ICP-MS determinations, and staff of the analytical center of Geological Institute of the Kola Research Center of the Russian Academy of Sciences, Apatity, Russia and especially its leader Dr. T.B. Bayanova for Sm-Nd isotope measurements.

REFERENCES

- Abdel-Rahman, A., 1994. Nature of biotites from alkaline, calc-alkaline, and peraluminous magmas. *Journal of Petrology*, 35(2), 525-541.
- Akinin, V.V. and Miller, E.L., 2011. Evolution of calc-alkaline magmas of the Okhotsk–Chukotka volcanic belt. *Petrology*, 19(3), 237–277.
- Al'Mukhamedov, A.I., Medvedev, A.Y. and Kirda, N.P., 1999. Comparative analysis of geodynamic settings of the Permo-Triassic magmatism in East Siberia and West Siberia. *Russian Geology and Geophysics*, 40(11), 1550-1561.
- Al'Mukhamedov, A.I., Medvedev, A.Y. and Zolotukhin, V.V., 2004. Chemical evolution of the Permian-Triassic basalts of the Siberian platform in space and time. *Petrology*, 12(4), 297-311.
- Amato, J.M. and Wright, J.E., 1997. Potassic mafic magmatism in the Kigluaik gneiss dome, northern Alaska: a geochemical study of arc magmatism in an extensional tectonic setting. *Journal of Geophysical Research*, 102, 8065-8084.
- Amato, J.M., Miller, E.L., Wright, J.E. and McIntosh W.C., 2003. Dike swarms on Seward Peninsula, Alaska, and their implication for kinematics of the Cretaceous extension in the Bering Strait region. *Canadian Journal of Earth Science*, 40, 865-886.
- Amato, J.M., Toro, J., Miller, E.L., Gehrels, G.E., Farmer, G.L. Gottlieb, E.S. and Till, A.B., 2009. Late Proterozoic-Paleozoic evolution of the Arctic Alaska-Chukotka terrane based

- on U-Pb igneous and detrital zircon ages: Implications for Neoproterozoic paleogeographic reconstructions. *GSA Bulletin*, 121(9/10), 1219–1235.
- Anderson, D.J., Lindsley, D.H. and Davidson, P.M., 1993. QUILF: a PASCAL program to access equilibrium among Fe-Mg-Mn-Ti oxides, pyroxenes, olivine and quartz. *Computers and geosciences*, 19, 1333-1350.
- Bayanova, T.B., 2004. Age of reference geological complexes of the Kola region and duration of magmatic processes. Nauka, St. Petersburg (in Russian).
- Bering Strait Geologic Field Party, 1997. Koolen metamorphic complex, NE Russia: implications for tectonic evolution of the Bering Strait region. *Tectonics*, 16, 713–729.
- Cabanis, B. and Lecolle, M., 1989. Le diagramme La/10-Y/15-Nb/8: un outil pour la discrimination des series volcaniques et la mise en evidence des processus de mélange et/ou de contamination crustale. *Comptes Rendus de l'Académie des Sciences. Series II*, 309, 2032-2029.
- Cecile, M.P., Lane, L.S., Khudoley, A.K. and Kos'ko M.K., 1999. Lower Paleozoic rocks around today's Arctic Ocean: two ancestral continents and associated plates; Alaskan rotation unnecessary and unlikely. *Polarforschung*, 69, 235- 241.
- Degtyaryov, V.S., 1975. Petrochemical peculiarities of the Amguema-Anyui diabase formation of the Chukotka fold region. In Shatalov, E.T. (ed.). *Magmatism of North East Asia*, part 2. Magadan book publisher, Magadan, 160-175 (in Russian).
- Dobretsov, N.L., Kirdyashkin, A.A., Kirdyashkin, A.G., Vernikovskiy, V.A. and Gladkov, I.N., 2008. Modeling of thermochemical plumes and implications for the origin of the Siberian traps. *Lithos*, 100, 66-92.
- Dorofeev, V. K., Blagoveschensky, M. G., Smirnov, A. N. and Ushakov, V. I., 1999. New Siberian Islands, geology and minerageny. *VNIIOkeangeologia*, Saint-Petersburg, 1-130 (in Russian).
- Fujita, K. and Newberry, J. T., 1982. Tectonic evolution of Northeastern Siberia and adjacent regions. *Tectonophysics*, 89, 337–357.
- Gel'man, M. L., 1963. Triassic diabase association in the Anyui fold zone (Chukotka). *Geologiya i Geofizika*, 2, 127-134 (in Russian).
- Govindaraju, K., 1994. 1994 compilation of working values and sample description for 383 geostandards. *Geostandards Newsletter*, 18 (Special Issue), 1–158.
- Grantz, A., May, S.D., Taylor, P.T. and Lawver, L.A., 1990. Canada Basin. In Grantz, A., Johnson, L. and Sweeney, J. F. *The Geology of North America*, vol. L: The Arctic Ocean Region. The Geological Society of America, Boulder, Colo, 379-402.
- Hofmann, A.W., 1988. Chemical differentiation of the Earth: the relationship between mantle, continental crust, and oceanic crust. *Earth and Planetary Science Letters*, 90, 297-314.
- Holland, T. and Blundy, J., 1994. Non-ideal interactions in calcic amphiboles and their bearing on amphibole-plagioclase thermometry. *Contributions to Mineralogy and Petrology*, 116, 433-47.
- Ivanov, O.N. and Milov, A.P., 1975. The diabase association in the Chukchi fold system and its relation to the basic magmatism in the northern portion of the Pacific Mobile Belt. In Shatalov, E.T. (ed.). *Magmatism of North East Asia*, part 2. Magadan book publisher, Magadan, 155-159 (in Russian).
- Kelemen, P.B., Hanghøj, K. and Greene, A.R., 2003. One view of the geochemistry of subduction-related magmatic arcs, with an emphasis on primitive andesite and lower crust. In Rudnick, R.L. (ed.). *The Crust*. Holland, H.D. and Turekian, K.K. (eds.) *Treatise on Geochemistry*, Volume 3. Elsevier-Pergamon, Oxford, 593–659.
- Krivolutskaya, N.A., 2013. Evolution of trap magmatism and origin of Pt-Cu-Ni ores of the Noril'sk province. Association of scientific publishers of KMK. 301 pp.
- Kuz'michov, A.B. and Pease, V.L., 2007. Siberian trap magmatism on the New Siberian Islands: constraints for Arctic Mesozoic plate tectonic reconstructions. *Journal of Geological Society*, 164, 959–968.
- Lanphere, M.A. and Dalrymple, G.B., 2000. First-principles calibration of ³⁸Ar tracers:

- Implications for the ages of $^{40}\text{Ar}/^{39}\text{Ar}$ fluence monitors. U.S. Geological Survey Professional Paper 1621, 10 p.
- Lawver, L.A. and Scotese, C.R., 1990. A review of tectonic models for the evolution of the Canada Basin. In: Grantz, A., Johnson, L. and J.F. Sweeney (eds.). *The geology of North America*, Geological Society of America, Boulder, Colorado, L (The Arctic Ocean Region), 593–618.
- Lawver, L.A., Grantz, A. and Gahagan, L.M., 2002. Plate kinematic evolution of the present Arctic region since the Ordovician. In: Miller, E.L., Grantz, A. and S.L. Klempere (eds.). *Tectonic evolution of the Bering shelf – Chukotka sea – Arctic margin and adjacent landmasses*. Geological Society of America, Special Paper 360, 333–358.
- Layer, P.W., 2000. Argon-40/argon-39 age of the El'gygytgyn impact event, Chukotka, Russia. *Meteoritics & Planetary Science*, 35, 591–599.
- Layer, P.W., Hall, C.M. and York, D., 1987. The derivation of $^{40}\text{Ar}/^{39}\text{Ar}$ age spectra of single grains of hornblende and biotite by laser step heating. *Geophysical Research Letters*, 14, 757–760.
- Layer, P.W., Newberry, R., Fujita, K., Parfenov, L., Trunilina, V. and Bakharev, A., 2001. Tectonic setting of the plutonic belts of Yakutia, northeast Russia, based on $^{39}\text{Ar}/^{40}\text{Ar}$ geochronology and trace element geochemistry. *Geology*, 29(2), 167–170.
- Leake, B.E., Woolley, A.R., Arps, C.S., Birch, W.D., Gilbert, M.C., Grice, J.D., Hawthorne, F.C., Kato, A., Kisch, H.J., Krivovichev, V. G., Linthout, K., Laird, J., Mandarino, J. A., Maresch, W.V., Nickel, E. H., Rock, N.M.S., Schumacher, J.C., Smith, D.C., Stephenson, N.C.N., Ungaretti, L., Whittaker, E.J.W. and Youzhi, G., 1997. Nomenclature of amphiboles: Report of the subcommittee on amphiboles of the international mineralogical association, commission on new minerals and mineral names. *The Canadian Mineralogist*, 35, 219–246.
- Ledneva, G.V., Sokolov, S.D. and Pease, V.L., 2011. Permo-Triassic hypabyssal mafic intrusions and associated tholeiitic basalts of the Kolyuchinskaya Bay, Chukotka (NE Russia): Links to the Siberian LIP. *Journal of Asian Earth Sciences*, 40, 737–745.
- LeMaitre, R.W., Bateman, P., Dudek, A., Keller, J., Lameyre, J., Le Bas, M.J., Sabine, P.A., Schmidt, R., Sorensen, H., Streckeisen, A., Woolley, A.R. and Zanettin, B., 1989. *A Classification of igneous rocks and glossary of terms: recommendations of the International Union of Geological Sciences Subcommittee on the systematics of igneous rocks*. Blackwell Scientific Publications, Oxford, U.K. 193 p.
- Lightfoot, P.C., Hawkesworth, C.J., Hergt, J., Naldrett, A.J., Gorbachev, N.S., Fedorenko, A.V. and Doherty, W., 1993. Remobilization of continental lithosphere by a mantle plume: major-trace-element, and Sr-, Nd- and Pb-isotopic evidence from picritic and tholeiitic lavas of the Noril'sk District, Siberian Trap, Russia. *Contributions to Mineralogy and Petrology*, 114, 171–188.
- McDougall, I. and Harrison, T.M., 1999. *Geochronology and thermochronology by the $^{40}\text{Ar}/^{39}\text{Ar}$ method-2nd ed*, Oxford University Press, New York, 269 pp.
- Medvedev, A.Ya., 2004. Permo-Triassic volcanism of the North Siberian craton (West Siberian Basin and Tunguska syncline): geochemistry, petrology and geodynamics. Doctor's thesis. Irkutsk, A.P. Vinogradov Institute of geochemistry, 306 pp (in Russian).
- Middlemost, A. K., 1994. Naming materials in the magma/igneous rock system. *Earth Science Review*, 37, 215–224.
- Miller, E. L., Katkov, S.M., Strickland, A., Toro, J., Akinin, V.V. and Dumitru, T.A., 2009. Geochronology and thermochronology of Cretaceous plutons and metamorphic country rocks, Anyui-Chukotka fold belt, North East Arctic Russia Stephan Mueller Special Publication Series, 4, 157–175.
- Miller, E.L., Toro, J., Gehrels, G., Amato, J.M., Prokopiev, A., Tuchkova, M.I., Akinin, V.V., Dumitru, T.A., Moore, T.E. and Cecile, M.P., 2006. New insights into Arctic paleogeography and tectonics from U–Pb detrital zircon geochronology. *Tectonics*, 25, 1–19.
- Nalivkin, D.V. (Ed.), 1983. *Geologic map of USSR*

- and adjacent aquatories. Scale 1:2500000. VSEGEI, St. Petersburg.
- Natal'in, B.A., Amato, J.M., Toro, J. and Wright, J.E., 1999. Paleozoic rocks of northern Chukotka Peninsula, Russian Far East: implication for the tectonics of the Arctic region. *Tectonics*, 18, 977–1003.
- Neal, C.R., Mahoney, J.J. and Chazey III, W.J., 2002. Mantle sources and the highly variable role of continental lithosphere in basalt petrogenesis of the Kerguelen plateau and Broken Ridge LIP: results from ODP Leg 183. *Journal of Petrology* 43, 1177–1205.
- Nokleberg, W.J., West, T.D., Dawson, K.M., Shpikerman, V.I., Bundtzen, T.K., Parfenov, L.M., Monger, J.W.H., Ratkin, V.V., Baranov, B.V., Byalobzhesky, S.G., Diggles, M.F., Eremin, R.A., Fujita, K., Gordey, S.P., Gorodinskiy, M.E., Goryachev, N.A., Feeney, T.D., Frolov, Y.F., Grantz, A., Khanchuck, A.I., Koch, R.D., Natal'in, B.A., Natapov, L.M., Norton, I.O., Patton Jr., W.W., Plafker, G., Pozdeev, A.I., Rozenblum, I.S., Scholl, D.W., Sokolov, S.D., Sosunov, G.M., Stone, D.B., Tabor, R.W., Tsukanov, N.V. and Vallier, T.L., 1998. Summary terrane, mineral deposit, and metallogenic belt maps of the Russian Far East, Alaska, and the Canadian Cordillera. US Geological Survey Open-File Report, 98–136.
- Parfenov, L.M., 1984. Continental margins and island arcs in the Mesozooids of Northeastern Asia. Nauka Publisher, Novosibirsk, 192 pp. (in Russian).
- Parfenov, L.M., Natapov, L.M., Sokolov, S.D. and Tsukanov, N.V. 1993. Terrane analysis and accretion in northeast Asia. *The Island Arc*, 2, 35–54.
- Pearce, J.A., 2008. Geochemical fingerprinting of oceanic basalts with applications to ophiolite classification and the search for Archean oceanic crust. *Lithos*, 100, 14–48.
- Putirka, K. D., 2008. Thermometers and barometers for volcanic systems. In: Putirka, K. D. and Tepley, F. (eds.). *Review in Mineralogy and Geochemistry*, 69, 61-120.
- Reichow, M.K., Pringle, M.S., Al'Mukhamedov, A.I., Allen, M.B., Andreichev, V.L., Buslov, M.M., Davies, C.E., Fedoseev, G.S., Fitton, J.G., Inger, S., Medvedev, A.Ya., Mitchell, C., Puchkov, V.N., Safonova, I.Yu., Scott, R.A. and Sauders, A.D. 2009. The timing and extent of the eruption of the Siberian traps large igneous province: Implication for the end-Permian environmental crisis. *Earth and Planetary Science Letters*, 277(1–2), 9–20.
- Ridolfi, F., Runzelli, A. and Puerini, M., 2009. Stability and chemical equilibrium of amphibole in calc-alkaline magmas: an overview, new thermobarometric formulations and application to subduction-related volcanoes. *Contribution to Mineralogy and Petrology*, 160(1), 45-66.
- Rudnick, R.L., and Fountain, D.M., 1995. Nature and composition of the continental crust: a lower crustal perspective. *Reviews of Geophysics*, 33, 267–309.
- Samson, S. D. and Alexander E. C., 1987. Calibration of the interlaboratory $^{40}\text{Ar}/^{39}\text{Ar}$ dating standard. *MMhb1: Chemical Geology*, 66, 27-34.
- Schmidt, M. W., 1992. Amphibole composition in tonalite as a function of pressure: an experimental calibration of the Al-in-hornblende barometer. *Contributions to Mineralogy and Petrology*, 110, 304-10.
- Seslavinsky, K.B., 1979. The South Anyui Suture (Western Chukotka). *Doklady Akademii Nauk SSSR*, 249, 1181–1185 (in Russian).
- Sokolov, S.D., Ledneva, G.V. and Pease, V.L., 2009. New data on the age and genesis of igneous rocks in the Kolyuchinskaya Guba (Eastern Chukotka). *Transactions (Doklady) of the Russian Academy of Sciences/Earth Science Section*, 425A(3), 384-388.
- Steiger, R. H. and Jaeger, E., 1977. Subcommittee on geochronology: convention on the use of decay constants in geo- and cosmochemistry. *Earth and Planetary Science Letters*, 36, 359–362.
- Streckeisen, A.L., 1974. Classification and nomenclature of plutonic rocks. Recommendations of the IUGS subcommission on the systematics of igneous rocks. *Geologische Rundschau. Internationale Zeitschrift für Geologie*. Stuttgart, 63, 773-785.
- Streckeisen, A.L., 1976. To each plutonic rock its proper name. *Earth Science Reviews*, 12, 1–33.
- Sun, S.S., and McDonough, W.F., 1989. Chemical

- and isotopic systematics of oceanic basalts: implication for mantle composition and processes. In: Saunders, A.D. and Norry, M.J. (Eds.), *Magmatism in the Oceanic Basins*. Geological Society Special Publication, 42, 313–345.
- Taylor, S.R. and McLennan, S.M., 1985. *The continental crust: Its composition and evolution*. Blackwell, Oxford, 312 pp.
- Tikhomirov, P.L., Kalinina, E.A., Moriguti, T., Makishima, A., Kobayashi, K., Cherepanova, I.Yu. and Nakamura, E., 2012. The Cretaceous Okhotsk–Chukotka Volcanic Belt (NE Russia): Geology, geochronology, magma output rates, and implications on the genesis of silicic LIPs. *Journal of Volcanology and Geothermal Research*, 221, 14–32.
- Tikhomirov, P.L., Luchitskaya, M.V. and Kravchenko-Berezhnoy, I.R., 2009. Comparison of Cretaceous granitoids of the Chaun tectonic zone to those of the Taigonos Peninsula, NE Asia: rock chemistry, composition of rock forming minerals, and conditions of formation. *Stephan Mueller Special Publication Series*, 4, 289–311.
- Til'man, S.M. and Sosunov, G.M. 1960. Some peculiarities of evolution of the Chukotka geosynclines in the Early Triassic. *Doklady Akademii Nauk SSSR*, 130(4), 834–837 (in Russian).
- Tuchkova, M.I., Sokolov, S. and Kravchenko-Berezhnoy, I.R., 2009. Provenance analysis and tectonic setting of the Triassic clastic deposits in Western Chukotka, Northeast Russia. *Stephan Mueller Special Publication Series*, 4, 177–200.
- Tynankergav, G.A. and Bychkov, J.M., 1987. Upper Triassic chert-volcanic-terrigenous assemblages of western Chukotka. *Doklady Akademii Nauk USSR* 296, 698–700 (In Russian)
- Vatrushkina, E.V. and Tuchkova M.I., 2014. Peculiarities of lithology and geochemistry of the Raucha Formation (upper Jurassic, western Chukotka). *Bulletin MOIP. Geology Branch* 89(1), 59–74 (in Russian).
- Vernikovskiy, V.A., Pease V.L., Vernikovskaya A.E., Romanov A.P., Gee D. and Travin, A.V., 2003. First report of early Triassic A-type granite and syenite intrusions from Taimyr: product of the northern Eurasian superplume? *Lithos*, 66(1–2), 23–36.
- Wood, D.A., 1980. The application of a Th-Ta-Hf diagram to problems of tectonomagmatic classification and to establishing the nature of crustal contamination of basaltic lavas of the British Tertiary volcanic province. *Earth and Planetary Science Letters*, 50, 11–30.
- Wooden, J.L., Czamanske, G.K., Fedorenko, V.A., Arndt, N.T., Chauvel, C., Bouse, R.M., King, B.W., Knight, R.J. and Siems, D.F., 1993. Isotopic and trace element constrains on mantle and crustal contributions to Siberian continental flood basalts, Noril'sk area, Siberia. *Geochemica et Cosmochemica Acta*, 57, 3677–3704.
- York, D., Hall, C.M., Yanase, Y., Hanes, J.A. and Kenyon, W.J., 1981. $^{40}\text{Ar}/^{39}\text{Ar}$ dating of terrestrial minerals with a continuous laser, *Geophysical Research Letters*, 8, 1136–1138.
- Zlobin, S. K. and Zakariadze, G. S., 1993. Composition and geodynamic setting of the plutonic series of ophiolites in the Sevan–Akerin zone (Lesser Caucasus). *Petrologiya*, 1, 413–430.

APPENDIX

Trace element contents in fractionated melt can in general be evaluated based on the Rayleigh fractionation model. Contents of major elements in melts can be evaluated using either the Rayleigh fractionation model or empirical correlations. However, both approaches have some limitations. Relationships between contents and activities of major elements deviate from Henry's law. Empirical correlations are not definite because any correlation can be described by different equations (especially when data are limited). Both these approaches are valid only for a restricted interval of fractionation, which is characterized by crystallization of a certain mineral assemblage and only limited variations of bulk element distribution coefficients.

According to the Rayleigh fractionation model, content of a trace element at a given degree of fractionation can be calculated using the equation

$$C=C_0*(1-xF)^{(KD-1)} \quad (1)$$

where KD is a bulk distribution coefficient (cumulate/melt) of an element, xF is a degree of fractionation (xF=0 for an initial melt), C₀ is a content of an element in an initial melt, C is a content of an element in fractionated melt. Correspondingly, values of xF can be estimated using an equation

$$xF=1-(C/C_0)^{(1/(KD-1))} \quad (2)$$

if values of C, C₀ and KD of a trace element are known. However, in our case compositions of actual rocks (Table 4) differ from compositions of melts due to a probable admixture of cumulative Fe-Ti oxides and a loss/gain of some major components during the rock metamorphism. Hence a content of an element in melt is related to its actual content in a rock as

$$C=C_{meas}*k, \quad (3)$$

where

$$k=100*(SiO_2+TiO_2+Al_2O_3+FeO^*+MnO+MgO+CaO+Na_2O+K_2O+Cr_2O_3+P_2O_5) \quad (4),$$

where contents of all oxides (wt. %) should correspond to their probable contents in a melt. This means that bulk rock contents of TiO₂, FeO*, MnO should be corrected to exclude the effect of an admixture of Fe-Ti oxides, and bulk rock contents of CaO, Na₂O and K₂O should be corrected to eliminate effects of element mobility (loss/gain) during metamorphism.

Additionally, values of KD for trace and major elements are not exactly known. However, one can infer from equation (1) that contents of two elements x and y in melts should correlate as

$$C_x/C_y=(C_{x_0}/C_{y_0})*(1-xF)^{(KD_x-KD_y)} \quad (5),$$

so that the content of an element is related with a the content of another element as

$$C_x=C_y*k_1*(1-xF)^{k_2} \quad (6).$$

The values k₁ and k₂ can be estimated for any two elements by a least square minimization procedure of actual-calculated C_x/C_y values for a number of cogenetic melts for which C_x, C_y and xF are known.

When two elements have a similar degree of compatibility, the equation (6) can be reduced to the form

$$C_x=C_y*k_1 \quad (7)$$

With a simple linear correlation between C_x and C_y.

Assuming a rock studied is a mixture of an initial melt fractionated to a certain degree and cumulative Fe-Ti oxides, the contents of FeO*, TiO₂, MnO, V and Nb in melts should correlate with contents of other elements. The correlations can be evaluated from compositions of 7 samples of the gabbro and diorite with the lowest TiO₂ contents which are assumed to be free of or contain only a little admixed Fe-Ti oxides. We prefer to use an average estimation based on values calculated using different element pairs (Table A1) in order to minimize both errors related to the deviation of iron behavior from Henry's law and analytical errors.

For evaluation of TiO₂ contents in melts at

different stages of fractionation we use correlation $TiO_2/SiO_2 - Gd/SiO_2$ (Fig. 10), correlation $TiO_2 - SiO_2$ and correlation $TiO_2 - Al_2O_3$:

$$TiO_2 = (0.0537 - 0.0302 * Gd/SiO_2) * SiO_2 \quad (8),$$

$$TiO_2 = SiO_2 * 0.0519 * (1 - xF)^{0.0901} \quad (9),$$

$$TiO_2 = Al_2O_3 * 0.182 * (1 - xF)^{-0.169} \quad (10),$$

where oxides are in wt.%, Gd (and other elements in equations below) in ppm, and xF is relative degree of crystallization. The form of equation (8) is empirical, and the form of equations (9) and (10) corresponds to the Rayleigh fractionation model.

Similarly, FeO* contents in melts can be calculated from compositions of the same reference rocks:

$$FeO^* = SiO_2 * 0.268 * (1 - xF)^{-0.0299} \quad (11),$$

$$FeO^* = Al_2O_3 * 0.931 * (1 - xF)^{-0.304} \quad (12),$$

$$FeO^* = MgO * 2.21 * (1 - xF)^{-0.962} \quad (13),$$

$$FeO^* = CaO * 1.26 * (1 - xF)^{-0.555} \quad (14).$$

In equation (14) CaO contents calculated by equations (33-35) were used in order to increase the accuracy of calculations.

Contents of MnO in melts were calculated using equations

$$MnO = SiO_2 * 0.00353 * (1 - xF)^{0.123} \quad (15),$$

$$MnO = Al_2O_3 * 0.0122 * (1 - xF)^{-0.158} \quad (16),$$

$$MnO = P_2O_5 * 0.582 * (1 - xF)^{0.918} \quad (17).$$

For calculation of V content in melts, we used equations

$$V = SiO_2 * 9.335 * (1 - xF)^{1.288} \quad (18),$$

$$V = Al_2O_3 * 33.2 * (1 - xF)^{1.090} \quad (19),$$

$$V = P_2O_5 * 1484 * (1 - xF)^{1.900} \quad (20).$$

Contents of Nb in melts were constrained using equations

$$Nb = SiO_2 * 0.305 * (1 - xF)^{-0.744} \quad (21),$$

$$Nb = Al_2O_3 * 1.058 * (1 - xF)^{-1.022} \quad (22),$$

$$Nb = Y * 0.355 * (1 - xF)^{-0.027} \quad (23),$$

$$Nb = P_2O_5 * 48.3 * (1 - xF)^{0.001} \quad (24),$$

$$Nb = La * 0.794 * (1 - xF)^{0.094} \quad (25),$$

$$Nb = Ce * 0.341 * (1 - xF)^{0.113} \quad (26).$$

Initial contents of K_2O , Na_2O and CaO in some investigated rocks seem to have changed during metamorphism (Fig. 12). However, contents of these components remain probably unchanged in a number of rocks, and this allows calculations of their initial contents in allochemically metamorphosed rock using an approach outlined above.

For potassium, using 5 rocks as reference ones (Fig. 12c),

$$K_2O = La * 0.0466 * (1 - xF)^{0.0203} \quad (27),$$

$$K_2O = Ce * 0.0199 * (1 - xF)^{0.0268} \quad (28),$$

$$K_2O = P_2O_5 * 2.72 * (1 - xF)^{-0.153} \quad (29).$$

For sodium, using 11 rocks as reference ones (Fig. 12b),

$$Na_2O = SiO_2 * 0.0567 * (1 - xF)^{0.101} \quad (30),$$

$$Na_2O = Al_2O_3 * 0.205 * (1 - xF)^{-0.144} \quad (31),$$

$$Na_2O = CaO * 0.260 * (1 - xF)^{-0.446} \quad (32).$$

In equation (32) CaO contents calculated by equations (33-35) were used in order to increase the accuracy of calculations for rocks probably experienced calcium gain/loss during metamorphism.

For calcium, using 7 rocks as reference rocks (Fig. 12a),

$$\text{CaO}=\text{SiO}_2*0.218*(1-\text{xF})^{0.519} \quad (33),$$

$$\text{CaO}=\text{Al}_2\text{O}_3*0.791*(1-\text{xF})^{0.279} \quad (34),$$

$$\text{CaO}=\text{MgO}*1.592*(1-\text{xF})^{-0.423} \quad (35).$$

At the first stage of the calculation, we estimated approximate xF (equation 2) for each rock assuming KD=0 for the most incompatible elements in cogenetic differentiated melts; in our case such elements are La and Ce. Then we calculated contents of the major elements in melts (using equations similar to 8-35). As major element contents in melts influence values of xF (equations 2-4) the calculation requires several iteration steps. Shown in equations 8-35 the values of coefficients reflecting the last step of the iteration procedure as well as the values of xF are listed in Table A1. Final contents of oxides and elements calculated using equations (8-35) along with average estimations are also presented in Table A1.

Table A1. Evaluation of relative degree of differentiation and elimination of effects of metamorphic loss/gain of some elements and cumulative Fe-Ti oxide admixture to melts.

#	1	2	3	4	5	6	7	8	9	10	11	12
Oxide/element	x _F	x _F [*]	x _F [*]	x _F [*]	TiO ₂	FeO [*]	FeO [*]					
Sample	calc	calc	calc	calc	actual	calc.	calc.	calc.	calc.	calc.	actual	calc.
	avg	us. La	us.Ce	avg		eqn.(8)	eqn.(9)	eqn.(10)	avg	excess		eqn.(11)
GY9-101	0.042	0.050	0.034	0.042	2.35	2.57	2.54	2.45	2.52	-0.17	12.79	13.22
PS9-92	0.197	0.209	0.186	0.197	2.58	2.51	2.47	2.60	2.53	0.06	13.31	13.12
GY9-74	0.000	0.000	0.000	0.000	6.17	2.21	2.21	2.06	2.16	4.01	18.33	11.41
GY9-79	0.040	0.041	0.039	0.040	5.28	2.28	2.27	2.11	2.22	3.06	16.82	11.80
KE9-71	0.107	0.106	0.105	0.105	5.72	2.32	2.31	2.38	2.34	3.39	16.43	12.12
PS9-89	0.207	0.211	0.201	0.206	3.82	2.43	2.40	2.40	2.41	1.42	15.77	12.75
KE9-73	0.113	0.112	0.115	0.114	5.98	2.30	2.29	2.32	2.30	3.68	17.11	12.01
GY9-99	0.425	0.427	0.427	0.427	3.59	2.08	2.08	2.08	2.08	1.51	21.53	11.47
GY9-81	0.439	0.442	0.434	0.438	4.62	2.32	2.31	2.38	2.34	2.29	17.55	12.78
GY9-102	0.440	0.441	0.438	0.440	3.38	2.36	2.34	2.46	2.39	0.99	16.33	12.97
PS9-90	0.494	0.497	0.491	0.494	3.24	2.43	2.39	2.53	2.45	0.79	15.69	13.42
GY9-76	0.520	0.516	0.524	0.520	4.31	2.40	2.39	2.19	2.33	1.98	17.27	13.51
GY9-82a	0.543	0.543	0.545	0.544	2.91	2.58	2.55	2.62	2.58	0.32	15.47	14.49
GY9-78	0.667	0.672	0.665	0.668	2.56	2.60	2.61	2.67	2.63	-0.06	13.47	15.40
GY9-82b	0.677	0.678	0.678	0.678	2.63	2.57	2.57	2.56	2.57	0.07	14.62	15.23
GY9-87	0.681	0.680	0.680	0.680	2.26	2.52	2.56	2.42	2.50	-0.24	15.77	15.21
GY9-84	0.669	0.666	0.670	0.668	2.55	2.51	2.54	2.52	2.53	0.03	16.20	15.02

Table A1. (continued)

#	13	14	15	16	17	18	19	20	21	22	23	24
Oxide/element	FeO [*]	MnO	MnO	MnO	MnO	MnO	MnO	V				
Sample	calc.	Calc.	Calc.	Calc.	Calc.	Actual	calc.	Calc.	Calc.	Calc.	Calc.	Actual
	eqn.(12)	eqn.(13)	eqn.(14)	avg	excess		eqn.(15)	eqn.(16)	eqn.(17)	avg	excess	
GY9-101	12.62	13.79	13.21	13.21	-0.42	0.171	0.173	0.164	0.174	0.171	0.001	396
PS9-92	13.70	12.70	13.22	13.18	0.12	0.168	0.167	0.174	0.164	0.168	0.000	391
GY9-74	10.55	13.54	11.78	11.82	6.51	0.214	0.150	0.138	0.145	0.145	0.070	833
GY9-79	10.86	14.07	12.18	12.23	4.59	0.208	0.154	0.142	0.153	0.150	0.058	754
KE9-71	12.40	12.61	12.39	12.38	4.05	0.222	0.157	0.160	0.166	0.161	0.062	658
PS9-89	12.67	13.51	12.97	12.98	2.79	0.203	0.162	0.161	0.170	0.164	0.039	618
KE9-73	12.05	12.69	12.25	12.25	4.86	0.229	0.155	0.155	0.181	0.164	0.065	727
GY9-99	11.49	31.43	17.59	17.99		0.221	0.139	0.139	0.125	0.134	0.087	495
GY9-81	13.17	14.42	13.42	13.45	4.10	0.215	0.154	0.159	0.160	0.158	0.058	416
GY9-102	13.62	22.61	16.16	16.34		0.204	0.156	0.164	0.164	0.162	0.043	491
PS9-90	14.22	17.84	15.06	15.13	0.56	0.185	0.159	0.169	0.171	0.166	0.018	417
GY9-76	12.38	16.73	14.10	14.18	3.09	0.266	0.159	0.146	0.173	0.159	0.107	197
GY9-82a	14.91	14.93	14.77	14.77	0.70	0.171	0.169	0.174	0.170	0.171	0.000	227
GY9-78	15.87	15.99	15.72	15.75	-2.27	0.137	0.171	0.177	0.158	0.169	-0.032	136
GY9-82b	15.28	14.61	15.03	15.04	-0.42	0.142	0.169	0.170	0.159	0.166	-0.024	126
GY9-87	14.46	14.56	14.73	14.74	1.03	0.202	0.168	0.160	0.175	0.168	0.034	46
GY9-84	15.00	15.47	15.13	15.15	1.04	0.190	0.167	0.167	0.180	0.172	0.019	96

Table A1. (continued)

#	25	26	27	28	29	30	31	32	33	34	35	36
Oxide/element	V	V	V	V	V	Nb	Nb	Nb	Nb	Nb	Nb	Nb
Sample	calc.	calc.	calc.	calc.	calc.	actual	calc.	calc.	calc.	calc.	calc.	calc.
	eqn.(18)	eqn.(19)	eqn.(20)	avg	excess		eqn.(21)	eqn.(22)	eqn.(23)	eqn.(24)	eqn.(25)	eqn.(26)
GY9-101	435	424	426	428	-32	14.7	15.5	14.8	15.1	15.1	14.6	14.7
PS9-92	342	360	338	347	45	16.2	17.5	18.2	16.8	16.6	17.1	16.9
GY9-74	397	377	370	381	452	17.8	13.0	12.0	14.6	12.1	12.2	12.5
GY9-79	389	366	376	377	377	17.2	13.8	12.7	14.8	13.2	13.1	13.4
KE9-71	363	378	379	373	285	20.4	15.0	15.3	17.1	15.3	14.4	14.7
PS9-89	327	327	346	333	284	18.9	17.1	17.0	17.7	17.5	16.5	16.6
KE9-73	357	364	410	377	350	20.9	14.9	14.9	16.5	16.7	14.2	14.5
GY9-99	192	189	185	189	306	22.5	19.4	19.4	21.0	17.2	20.1	20.4
GY9-81	208	210	232	216	200	27.6	22.0	22.7	23.5	22.6	21.7	21.7
GY9-102	210	217	238	222	269	23.5	22.3	23.5	22.9	23.2	22.6	22.8
PS9-90	190	196	224	203	214	23.5	24.9	26.4	24.0	26.6	25.1	25.0
GY9-76	179	159	214	184	13	32.2	26.0	23.8	28.1	28.2	25.1	25.7
GY9-82a	179	179	201	186	41	32.8	28.9	29.7	28.2	29.0	29.0	29.3
GY9-78	126	122	137	128	8	38.1	38.5	39.7	38.2	35.9	38.9	38.1
GY9-82b	120	113	134	122	3	35.3	38.9	39.1	38.2	37.3	39.2	39.2
GY9-87	118	105	146	123	-77	40.2	39.1	37.3	40.4	41.3	39.4	39.4
GY9-84	122	115	156	131	-35	38.5	37.7	37.7	39.3	41.3	38.1	38.6

Table A1. (continued)

#	37	38	39	40	41	42	43	44	45	46	47	48
Oxide/element	Nb	Nb	K ₂ O	Na ₂ O	Na ₂ O	Na ₂ O	Na ₂ O					
Sample	calc.	calc.	actual	calc.	calc.	calc.	calc.	calc.	actual	calc.	calc.	calc.
	avg	excess		eqn.(27)	eqn.(28)	eqn.(29)	avg	loss		eqn.(30)	eqn.(31)	eqn.(32)
GY9-101	15.0	-0.2	0.72	0.86	0.86	0.85	0.86	0.14	2.55	2.78	2.76	2.84
PS9-92	17.2	-1.0	1.07	1.02	1.01	0.97	1.00	-0.07	3.68	2.70	2.91	2.87
GY9-74	12.7	5.0	0.47	0.72	0.73	0.68	0.71	0.23	2.48	2.41	2.32	2.41
GY9-79	13.5	3.7	0.38	0.77	0.78	0.75	0.77	0.39	2.44	2.48	2.37	2.57
KE9-71	15.3	5.1	0.80	0.85	0.87	0.88	0.87	0.06	2.66	2.53	2.68	2.67
PS9-89	17.1	1.8	0.99	0.99	0.99	1.02	1.00	0.00	3.05	2.62	2.69	2.72
KE9-73	15.3	5.6	0.61	0.84	0.86	0.96	0.89	0.28	2.42	2.50	2.60	2.50
GY9-99	19.6	2.9	0.43	1.24	1.25	1.05	1.18	0.75	1.84	2.26	2.31	2.35
GY9-81	22.4	5.2	1.06	1.34	1.33	1.39	1.35	0.29	2.70	2.51	2.64	2.60
GY9-102	22.9	0.6	1.09	1.39	1.40	1.43	1.41	0.32	2.20	2.54	2.73	2.71
PS9-90	25.3	-1.8	1.03	1.56	1.55	1.66	1.59	0.56	3.07	2.60	2.80	2.77
GY9-76	26.2	6.0	0.88	1.57	1.60	1.78	1.65	0.77	2.65	2.60	2.42	2.81
GY9-82a	29.0	3.8	1.88	1.82	1.83	1.84	1.83	-0.05	2.85	2.77	2.89	2.91
GY9-78	38.2	-0.1	0.79	2.50	2.44	2.39	2.45	1.66	4.04	2.82	2.93	2.95
GY9-82b	38.6	-3.3	2.46	2.53	2.52	2.50	2.52	0.06	2.67	2.78	2.81	2.87
GY9-87	39.5	0.7	1.52	2.54	2.54	2.78	2.62	1.10	2.70	2.77	2.65	2.79
GY9-84	38.8	-0.3	1.65	2.45	2.48	2.76	2.56	0.91	2.71	2.75	2.76	2.65

Table A1. (continued)

#	49	50	51	52	53	54	55	56
Oxide/element	Na ₂ O	Na ₂ O	CaO	CaO	CaO	CaO	CaO	CaO
Sample	calc.	calc.	actual	calc.	calc.	calc.	calc.	calc.
	avg	gain		eqn.(33)	eqn.(34)	eqn.(35)	avg	loss
GY9-101	2.77	-0.22	9.50	10.52	10.45	9.73	10.23	0.73
PS9-92	2.80	0.88	8.64	9.47	10.24	8.15	9.29	0.64
GY9-74	2.36	0.12	9.26	9.29	8.96	9.78	9.35	0.09
GY9-79	2.45	-0.01	9.70	9.40	9.01	9.94	9.45	-0.25
KE9-71	2.60	0.06	8.82	9.27	9.86	8.56	9.23	0.41
PS9-89	2.65	0.39	8.18	9.14	9.40	8.61	9.05	0.87
KE9-73	2.51	-0.09	9.13	9.16	9.55	8.59	9.10	-0.03
GY9-99	2.29	-0.44	6.52	6.89	7.06	16.83	10.26	
GY9-81	2.56	0.14	7.74	7.58	7.99	7.62	7.73	-0.01
GY9-102	2.64	-0.44	6.58	7.68	8.25	11.95	9.30	
PS9-90	2.70	0.37	7.06	7.52	8.11	8.92	8.18	1.12
GY9-76	2.59	0.07	7.79	7.35	6.85	8.13	7.44	-0.35
GY9-82a	2.83	0.02	4.42	7.67	8.02	7.07	7.58	3.16
GY9-78	2.88	1.16	5.43	6.85	7.09	6.38	6.78	1.34
GY9-82b	2.79	-0.12	4.91	6.67	6.71	5.74	6.37	1.46
GY9-87	2.71	-0.01	5.41	6.62	6.31	5.68	6.20	0.80
GY9-84	2.70	0.01	6.22	6.67	6.69	6.15	6.50	0.28

Notes to Table A1. Contents of major elements and trace elements are in wt. % and in ppm, respectively; data are not recalculated to a water-free base as it is in Table 4. x_F is an average value of a relative degree of differentiation of an initial melt (corresponds to sample GY9-74) calculated using La and Ce concentrations in rocks and used to evaluate contents of oxides and elements, which are shown in this Table. x_{F^*} is a value of a relative degree of differentiation of an initial melt (calculations using La, Ce and average) obtained at the next step of the iteration and demonstrating the that sufficiency sufficient of the iterations were done. A difference between $x_F(\text{La})$ and $x_F(\text{Ce})$ reflects an error of x_F calculation. “Excess” is a difference between an actual concentration of an oxide or an element in a rock and its average calculated content in a melt; “excess” probably reflects an amount of an oxide or an element in a rock related to an admixed cumulative Fe-Ti oxides. “Loss/Gain” is a difference between an actual content of an oxide or an element in a rock and its average calculated content in a melt. “Loss/Gain” reflects an amount of a component removed or added during allochemical metamorphism of a rock. The reference contents of oxides and elements are shown in bold. Contents of oxides and elements calculated using different equations are similar; it and indicates that our approaches are correct. In samples Gy9-99 and GY9-102 contents of CaO and FeO estimated using different equations significantly differ. It This can be attributed either to a significant amount of cumulative silicate phases (that were not taken into account in the calculations) or to allochemical behavior of some major elements (MgO?) in metamorphism (in rest of the samples MgO is probably inert in metamorphism).